HHS Public Access

Author manuscript

Neuron. Author manuscript; available in PMC 2021 September 09.

Published in final edited form as:

Neuron. 2020 September 09; 107(5): 782–804. doi:10.1016/j.neuron.2020.07.020.

Ultra-slow oscillations in fMRI and resting-state connectivity: Neuronal and vascular contributions and technical confounds

Patrick J. Drew[1,2,3,*], **Celine Mateo**[4,*], **Kevin L. Turner**[2], **Xin Yu**[5,6], **David Kleinfeld**[4,7,8]

[1]Department of Engineering Science and Mechanics, Pennsylvania State University, University Park, PA 16802, USA

[2]Department of Biomedical Engineering, Pennsylvania State University, University Park, PA 16802, USA

[3]Department of Neurosurgery, Pennsylvania State University, University Park, PA 16802, USA

[4]Department of Physics, University of California, San Diego, CA 92093 USA

[5]High-Field Magnetic Resonance Department, Max Planck Institute for Biological Cybernetics, 72076 Tuebingen, Germany

[6]MGH/MIT/HMS Athinoula A. Martinos Center for Biomedical Imaging, Department of Radiology, Harvard Medical School, Massachusetts General Hospital, Charlestown, MA 02114, USA

[7]Section of Neurobiology, University of California, San Diego, CA 92093 USA

[8]Lead author

Abstract

Ultra-slow, ~ 0.1 Hz variations in oxygenation level of brain blood is widely used as a fMRI-based surrogate of “resting-state” neuronal activity. The temporal correlations among these fluctuations across the brain are interpreted as “functional connections” for maps and neurological diagnostics. Ultra-slow variations in oxygenation follow a cascade. First, they closely track changes in arteriole diameter. Second, interpretable “functional connections” arise when the ultra-slow changes in amplitude of γ-band neuronal oscillations, which are shared across even far-flung but synaptically connected brain regions, entrain the ~ 0.1 Hz vasomotor oscillation in diameter of local arterioles. Significant confounds to estimates of “functional connectivity” arise from residual vasomotor activity as well as arteriole dynamics driven by self-generated movements and subcortical common modulatory inputs. Lastly, methodological limitations of fMRI can lead to spurious “functional connections”. The neuronal generator of ultra-slow variations in γ-band amplitude, including that associated with self-generated movements, remains an open issue.

Lead Contact: David Kleinfeld, University of California, 9500 Gilman Drive, La Jolla, CA 92093–0374, Phone: 858–822–0342, dk@physics.ucsd.edu.

*contributed equally

INTRODUCTION

How do brains compute? The answer to this question takes on many guises. It has proven useful to differentiate brain regions on the mesoscopic scale, i.e., as an average over large number of individual neurons, and thus define connections and signaling on the same mesoscopic scale (Mitra, 2014; Zeng, 2018). As an example, the flow of sensory input in the transformation from perception to action can be described as a flow from primary sensory areas to motor areas (Ferezou et al., 2007; Li et al., 2016). Mesoscopic connectivity diagrams are readily determined based on the histological analysis of tissue subsequent to the injection and transport of anterograde and/or retrograde markers (Bohland et al., 2009; Kim et al., 2017). However, the determination of connectivity within the living animal, and the modulation of signaling along established axonal pathways as a function of brain state, requires a noninvasive procedure. A well-established, albeit incompletely understood approach is based on functional magnetic resonance imaging (fMRI), an imaging modality that infers neuronal activity from changes in localized brain blood oxygenation (Logothetis and Wandell, 2004; Shulman et al., 2002).

Here we review the use of fMRI to infer neuronal connectivity between well separated regions in the forebrain. These are correlation-based methods, and regions with strong correlations between their resting-state signals are said to be “functionally connected”. Connected graphs that are comprised of regions as vertices and strong correlations as edges are said to form “default networks” of brain activity (Greicius et al., 2003; Raichle et al., 2001; Sporns et al., 2005). Such networks have been characterized in humans (De Luca et al., 2006; De Luca et al., 2005; Majeed et al., 2011; Zhao et al., 2008), monkeys (Shmuel and Leopold, 2008; Vincent et al., 2007), and rats (Gozzi and Schwarz, 2016; Lu et al., 2012; Majeed et al., 2011; Stafford et al., 2014; Thompson et al., 2013), albeit not without controversy as to reliability (Honey et al., 2009). Our review generally avoids the discussion of signals from anesthesia animals and humans in light of the strong disruption in the interaction between neurons and blood vessels by most anesthetic agents (Gao et al., 2017; Goense and Logothetis, 2008; Pisauro et al., 2013).

FUNDAMENTALS

Both the flow and oxygenation of blood in the brain is modulated by neuronal activity. This modulation forms the basis of fMRI and intrinsic optical signal (IOS) imaging. Two coupled effects are at work. First, an increase in neuronal activity will lead to an increase in the diameter of the pial arterioles that distribute blood to the brain. This change in diameter will long outlast the stimulus (Drew et al., 2011; Uhlirova et al., 2016) (Fig. 1A). Second, an increase in neuronal activity will initially lead to a decrease in blood oxygenation in the microvessels and veins, seen most prominently in the upper layers of cortex (Buxton, 2001; Grinvald et al., 1991; Tian et al., 2010), albeit this interpretation is not universally accepted (Şencan et al., 2020; Sirotin et al., 2009; Uludağ et al., 2009). The increase in oxygen consumption is soon overcompensated by an increase in blood flow and a concomitant increase in blood oxygenation. The overcompensation reflects the active nature of neurovascular coupling (Attwell et al., 2010; Cauli and Hamel, 2010; Iadecola, 2004; Kleinfeld et al., 2011). The overcompensation can localize to one or few cortical columns

(Grinvald et al., 1991), yet it may have a global component from dilation of arterioles caused by change in the activity of sympathetic input (Dacey Jr and Duling, 1984).

The oxygenation state of blood can be detected via differences in the electronic properties of oxy- versus deoxyhemoglobin. This is reported by a greater reflection of red light by oxy- versus deoxyhemoglobin, which is routinely detected by IOS imaging (Lieke et al., 1989) (Fig. 1B). It is also reported by a change from a diamagnetic to a paramagnetic state by oxy- versus deoxyhemoglobin, respectively (Pauling and Coryell, 1936). Thus, the magnetic susceptibility of capillary and venous blood is correlated with neuronal activity. The change in arteriole diameter and blood oxygenation are coupled; the overcompensation of blood oxygenation is quenched when the pial arterioles are fully dilated using isoflurane prior to the onset of neuronal activity (Fig. 1B) (Knutsen et al., 2016).

Communication from neurons to arteriole smooth muscle.

How do neurons communicate with arterioles? There are multiple mechanisms that neurons in the brain use to control their own supply of blood (Attwell et al., 2010; Cauli and Hamel, 2010; Iadecola, 2004; Kleinfeld et al., 2011). We review two mechanisms that acts on a < 1 s time-scale. The lumen of the blood vessels is formed by endothelial cells that are connected with relatively low resistance gap junctions, such that passive signaling occurs with an ~ 2 mm electrotonic length (Segal and Duling, 1989; Welsh et al., 2018). Further, the smooth muscle cells that drive vascular tone are in strong electrical contact with the endothelial cells. In the presence of bursts of neuronal spikes, there is an outflow of K^+ ions in the perivascular space (Caesar et al., 1999; Rasmussen et al., 2019). This can lead to regenerative, hyperpolarizing pulses that propagate along the endothelial cells from the subsurface microvessels to the penetrating arterioles (Longden et al., 2017) and then to pial arterioles (Fig. 1C). The hyperpolarization will spread to smooth muscle and dilate the pial arterioles (Filosa et al., 2006; Knot and Nelson, 1998) (insert in Fig. 1C). This sequence of activation is supported by the stimulus-driven progression in arteriole dilation from middle layers to the pia in cortex (Tian et al., 2010). While details of the conditions for passive versus active spread of signals in the pial network remain to be addressed (Harraz et al., 2018), direct electrical coupling through the endothelium provides a means for neurons to directly influence the diameter of neighboring arterioles (Fig. 1A).

Nitric oxide (NO) is a well-known vasodilator that is produced by nitric oxide synthase (NOS) in neurons and can act quickly to relax smooth muscle (Fig. 6). As a caveat, the role of NO as a transient actuator of change in arteriole dilation (Ma et al., 1996), as opposed to a co-factor in effecting change (Lindauer et al., 1999), remains unsettled (Attwell et al., 2010), though optogenetic stimulation of neurons that express NO-synthase will drive an increase in blood flow (Krawchuk et al., 2019). The role of astrocytes in the control of flow is also controversial (Kleinfeld et al., 2011; Mishra et al., 2016; Nizar et al., 2013; Rosenegger et al., 2015), with arteriole dilation occurring only in the presence of relative large signaling events by astrocytes (Schulz et al., 2012).

Background on fMRI.

The blood oxygenation level dependent (BOLD) fMRI signal exploits the shift in the magnetic properties of deoxyhemoglobin versus oxyhemoglobin (Villringer and Dirnagl, 1995). In practice, these are detected by changes to the relaxation time of water protons in the brain (Ogawa et al., 1993; Stephan et al., 2004). Longer relaxation times implies greater oxygenation and a larger BOLD fMRI signal. The BOLD effect was discovered in 1990 by Seiji Ogawa using anesthetized rats (Ogawa et al., 1990). Two years later, BOLD was independently demonstrated in the awake human brain by the laboratories of James Hyde (Bandettini et al., 1992), Bruce Rosen (Kwong et al., 1992) and Kamil Ugurbil (Ogawa et al., 1992). As an example, successive eye opening and closing in humans leads to a change in the BOLD fMRI signal in the brain region that corresponds to primary visual cortex (Fox and Raichle, 2007) (Fig. 2A). In terms of impact, the use of BOLD fMRI has stormed across the disciplines of psychology and cognitive neuroscience as a means to infer changes in neuronal activity during all aspects of cognitive tasks performed by humans.

A complementary technique, cerebral blood volume (CBV) fMRI, infers neuronal activity from an increase in total hemoglobin in response to neuronal activity. It was first demonstrated in the human brain using subjects whose blood was doped with gadolinium, a paramagnetic ion that vastly increases the magnetic susceptibility of blood (Belliveau et al., 1991; Kwong et al., 1992). The increase in blood volume is secondary to an increase in arteriole diameter (Fig. 1B). Subsequent work has demonstrated CBV fMRI using label-free procedures (Huber et al., 2017; Lu et al., 2003).

Noise and the determination of correlated brain activity.

The physicist Lewis Branscomb famously wrote "*God loves the noise as much as the signal*." (Branscomb, 1995). The noise in the fMRI signal, a part of physiological contributions such as breathing and technical noise, has dominant albeit broad spectral bands (Mitra and Bokil, 2008; Papoulis, 1962) near 0.1 Hz (Fig. 2B). The exact frequency can vary on the scale of centimeters across the human brain. Mindful of Branscomb's prescient comment, only a few years after the advent of BOLD fMRI, additional experiments in the laboratory of James Hyde showed that the variability observed in the BOLD fMRI signal is correlated across well-separated regions in the brain. The initial observations involved subregions in motor cortex of the two hemispheres whose BOLD fMRI signals co-fluctuate in the vicinity of 0.1 Hz in the absence of a task (Biswal et al., 1995). These signals, in contrast to stimulus- and task-based fMRI, are measured in the absence of a cognitive task or any overt stimulus and are referred to as resting-state fMRI signals (Biswal et al., 2010). They are thus referred to as the resting-state BOLD fMRI. In fact, the signal between any pair of well separated regions in the brain will co-fluctuate so long as they maintain long-range, i.e., white matter, connections (Fox et al., 2005). This is illustrated for resting-state BOLD fMRI signals from the posterior cingulate cortex (PCC) and medial prefrontal cortex (mPFC) (left and center, Fig. 2C), which are connected by a white matter tract along the cingulum bundle (Greicius et al., 2009) (right, Fig. 2C). In general, resting-state fMRI signals are particularly strong between regions in opposing hemispheres with mirrored neuronal activation (Smith et al., 2009) (Fig. 2D), albeit these signals are accompanied by brain-wide activation (Schölvinck et al., 2015).

Arteriole diameter naturally oscillates near 0.1 Hz.

What are physiological attributes of blood vessels that allow them to be coupled to ongoing neuronal activity in the absence of a task (Fig. 2C,D), as opposed to be driven by strong sensory stimuli (Fig. 1)? Further, what is the origin of the ~ 0.1 Hz frequency-scale for the ultra-slow dynamics that dominate the resting-state BOLD fMRI signal (Fig. 2B)? Both of these questions are answered by recalling that arteries undergo vasomotor oscillations as part of their normal physiology (Intaglietta, 1990). These are collective oscillations of contractile tone in the smooth muscle cells that surround arterioles and lead to rhythmic changes in arteriole diameter (Aalkjær et al., 2011; Intaglietta, 1990) that are referred to as vasomotion. The rhythm thought to be generated by the interactions of active conductances in the membranes of smooth muscle and endothelial cells (Aalkjaer and Nilsson, 2005; Haddock and Hill, 2005) with the mechanical forces generated by flow (Koenigsberger et al., 2006; Stergiopulos et al., 1998). Vasomotion occurs within a broad frequency band that is centered near 0.1 Hz in humans (Noordmans et al., 2018; Obrig et al., 2000; Rayshubskiy et al., 2013), mice (Drew et al., 2011), and rats (Kleinfeld et al., 1998; Mayhew et al., 1996). Vasomotor oscillations in arteriole diameter drive oscillations in the velocity of red blood cells in the microvessels (Drew et al., 2010; Kleinfeld et al., 1998) and changes in the partial pressure of oxygen in brain tissue (Mateo et al., 2017; Mayhew et al., 1996).

As an intrinsic property, vasomotor oscillations are observed in isolated brain arterioles that are cannulated, pressurized, and maintained at physiological temperature (Osol and Halpern, 1988) (Fig. 3A). Critically, vasomotion is observed in pial arterioles in vivo (left, Fig. 3B) and is only slightly reduced in amplitude, by a factor of 0.2, when cortical activity is silenced to isolate the vessels from ongoing cortical, albeit not sympathetic, neuronal activity (Winder et al., 2017) (center and right, Fig. 3B).

The presence of ultra-slow natural oscillations in the diameter of brain arterioles raises three questions. First, what is the relation of the oscillation to the change in oxygenation of the neighboring tissue, i.e., the parenchymal contribution to the BOLD signal? Simultaneous measurements of the arteriole diameter and the intrinsic optical signal in awake mice show that the two are strongly coherent (Mateo et al., 2017). The peak value of oxygenation lags the peak of vasodilation by ~ 1 s. The positive coupling of blood oxygenation with a change in arteriole diameter is consistent with the changes that occur upon sensory stimulation (Fig. 1).

The second question, given the coupling of blood oxygenation to vasomotion, concerns the spatial scale of synchronous vasomotor oscillations. The results from direct measurements of vessel diameter in awake rodents indicate that vessels within a radius of ~ 2 mm tend, on average, to dilate synchronously (Mateo et al., 2017). Further, since the radius is the only dimension of blood vessels that can change, CBV fMRI provides a measure of arteriole diameter. Using this technique with anesthetized rodents, a correlation length of ~ 2 mm is also reported (He et al., 2018). Thus, despite the short-range fall-off, are changes in diameter strongly coordinated across distant but mirrored regions in the two hemispheres (Fig. 3C)? Optical imaging data from rodents shows that such transhemispheric changes are strongly correlated (Mateo et al., 2017; Tsai et al., 2015). Similar results are inferred with CBV fMRI of the primate brain (Schölvinck et al., 2010). All told, mirrored regions in the two

hemispheres show synchronous oscillations in arteriole diameter (Fig. 3C) in addition to blood oxygenation (Fig. 2D).

The third question is how fast the callosal coupling between neurons in opposite hemispheres must be to support synchronous ultraslow activity. For the simplest models of weakly coupled oscillators, this means a delay of less than a quarter of a period (Sompolinsky et al., 1991; Yeung and Strogatz, 1999). This corresponds to ~ 2 s, which is two orders of magnitude longer than transhemispheric propagation delays. The arteriole vasomotion in each hemisphere is synchronous through the similarly delayed neuronal-to-vascular coupling (Fig. 1).

SOURCES OF ULTRA-SLOW ELECTRICAL SIGNALING TO COUPLE TO VASOMOTION

The theory of weakly coupled oscillators (Kuramoto, 1984) implies that vasomotor oscillations can phase-lock to rhythmic neuronal activity within the same ~ 0.1 Hz frequency band. We consider three such sources of activity (Fig. 4A). The first two involve ultra-slow variations in neuronal electrical potential. One realization is in terms of an ultra-slowly varying envelope of high-frequency electrical oscillations in the brain (Leopold et al., 2003; Nir et al., 2008; Thompson et al., 2013). A second is in terms of potential ultra-slow variations in the electrocorticogram (ECoG) or electroencephalogram (EEG) (He and Raichle, 2009). The ECoG and the EEG measure spatially extended and temporally coherent extracellular current flow in the brain (Lemon, 1984). The third potential source of ultra-slow rhythmic activity is via neuromodulator nuclei. We consider the viability of each of these signaling mechanisms as a prelude to describing the locking of vasomotor activity to ultra-slow electrical signal in the brain.

Ultra-slow electrical signaling by modulation of γ-band oscillations.

Gamma-band oscillations refer to rhythmic brain activity in a broad range of frequencies, typically 30 to 80 Hz. It can be generated in vitro by networks of solely fast-spiking inhibitory neurons (Whittington et al., 1995), consistent with theoretical predictions (Hansel et al., 1993; van Vreeswijk et al., 1994). In vivo, the details of the oscillatory waveform are shaped by the interactions between parvalbumin and pyramidal neurons (Cardin et al., 2009; Sohal et al., 2009) as well as by interactions with different classes of inhibitory neurons (White et al., 2000) and cholinergic modulation (Pinto et al., 2013).

A key feature of γ-band oscillations is that the amplitude, or equivalently the spectral power, can vary over time (Leopold et al., 2003; Liu and Duyn, 2013; Mateo et al., 2017; Nir et al., 2008; Thompson et al., 2013). In fact, an increase in power in the γ-band is a predictor of a subsequent increase in arteriole diameter and blood oxygenation (Mateo et al., 2017; Winder et al., 2017). Consistent with these physiological changes, there is a corpus of evidence that increased power in the γ-band correlates with an increase with the BOLD fMRI signal (Goense and Logothetis, 2008; Keller et al., 2013; Lachaux et al., 2007; Lima et al., 2014; Niessing et al., 2005; Nir et al., 2007; Schölvinck et al., 2010). While the power in the γ-band is the best predictor of an increase in arteriole diameter, the correlation with the

spectral power extends down to lower frequencies (Goense and Logothetis, 2008; Mateo et al., 2017; Winder et al.,2017).

As a matter of principle, amplitude modulation (Black, 1953) provides a means for ultra-slow signals to be transmitted in the brain, as can occur by modulating the interspike interval in a spike train by an inhomogeneous spike rate (Okun et al., 2019). Here, the γ-rhythm oscillations serve as the underlying carrier frequency and the broad-band, ~ 0.1 Hz rhythm modulates the amplitude of the γ-rhythm oscillations (Fig. 4B). The power spectrum of the γ-rhythm oscillations is broadened by the modulation but still centered at a high frequency; there is no spectral power at the broad-band, ~ 0.1 Hz modulation (Fig. 4B). Demodulation of the signal, which involves spectral mixing and can be accomplished by the threshold properties of neurons (Ahrens et al., 2002), retrieves the ultra-slow signal (Fig. 4B). Recent data from the mouse accessory olfactory bulb implies that ultra-slow modulation can be quite strong in practice (Tsitoura et al., 2020).

Evidence for encoding of ultra-slow oscillations by the modulation of γ-rhythm oscillations comes from studies on monkey (Leopold et al., 2003) and human subjects (Nir et al., 2008). The human study involved bilateral recordings of multi-unit spike waveforms and the ECoG from the parietal and temporal lobes of both cortices in preoperative patients. A spectrogram of the ECoG acquired while a subject was in non-REM sleep shows that the power in the γ-band is slowly modulated (Fig. 4C). The spectral power of the modulation in γ-band power. i.e., the so-called second spectrum, shows peaks at frequencies near 0.1 Hz (Drew et al., 2008) (Fig. 4C). These modulations are present during both states of sleep and states of wakefulness.

Is the modulation in γ-band power correlated across hemispheres, as would be expected if these signals relate to transhemispheric correlation in the BOLD fMRI signal (Fig. 2D) and the arteriole diameter (Fig. 3C)? The spike times at spatially adjacent regions as well as at functionally linked areas of opposing hemispheres are not coincident. In contrast, there is significant coherence in the modulation of the spike rate and in the power of γ-band oscillations in the ECoG across sites in opposing hemispheres (Nir et al., 2008). During rest, there is a relatively large and positive correlation coefficient of 0.6 between ultra-slow ECoG signals from contralateral auditory areas, as compared with smaller correlation coefficients between signals from auditory and nonauditory areas. The stimulus-linked synchrony between the auditory areas in opposite hemispheres is likely mediated through callosal connections (Engel et al., 1991). The literature therefore suggest that ~ 0.1 Hz signals are transmitted as modulation of the high frequency γ-band rhythm, which is coherent across mirrored regions in the two hemispheres.

A final concern is the spatial specificity of the ultra-slow modulation that forms correlated signals across hemispheres. This was addressed using wide-field optical imaging of the dorsal surface of cortex in transgenic mice that express functional indicators of intracellular calcium (Barson et al., 2019; Ma et al., 2016; Vanni et al., 2017) or transmembrane voltage (Chan et al., 2015; Mohajerani et al., 2013). These indicators report the accumulation of spiking activity, which approximates rectification of neuronal activity above a threshold level (Fig. 4B) and thus reports the ultra-slow envelope of neuronal activity. While strong

correlations occur for frequencies over the range from 0.1 Hz to 10 Hz, the amplitude of the oscillations across the dorsal surface is greatest in the 0.08 - 0.16 Hz frequency band, i.e., centered near 0.1 Hz, as opposed to bands below this frequency and up to 10 Hz (Vanni et al., 2017). Further, bilateral symmetry of the neuronal response is largely reduced in acallosal mice (Mohajerani et al., 2010), albeit this issue is not without controversy (Quigley et al., 2003; Tyszka et al., 2011).

Ultra-slow changes in the electrocorticogram report non-neuronal dynamics.

The EEG is traditionally recorded as surface potentials across the brain (Lemon, 1984). Ultra-slow variations in the ECoG or EEG, also referred to as “DC potentials”, are presumed to result from ultra-slow changes in active membrane currents (Besson et al., 1970) and are a complementary means to support ultra-slow neuronal activity to that of modulation of the high frequency γ-rhythm (Fig. 4B,C). Yet extensive experimental evidence has shown that EEG signals with spectral components below ~ 1 Hz have a non-neuronal origin. One mechanism to generate ultra-slow surface potentials is through changes in the volume of blood in the brain. The electrical potential of the blood is negative relative to that of the cerebrospinal fluid (Held et al., 1964; Sorensen and Severinghaus, 1970). Thus dilation of arterioles, which in the awake animal can take place over seconds, and dilation of veins, which can occur over tens of seconds (Drew et al., 2011; Huo et al., 2015; Pisauro et al., 2013), will generate ultra-slow changes in the EEG (Besson et al., 1970; Nita et al., 2004; Vanhataloa et al., 2003; Voipio et al., 2003) that are unrelated to neuronal activity per se.

Experiments on human subjects have shown that a shift in blood volume, driven by changes either in posture or breathing that are unlikely to induce significant neuronal effects, will drive ultra-slow changes in the EEG. In the Mueller maneuver, the subject attempts to inhale with their mouth closed and nostrils plugged. In the Valsalva maneuver, the subject attempts to exhale against a closed airway; this is a common means to equalize pressure to the sinuses. These procedures drive a change in blood volume, measured with near infrared spectroscopy (NIRS), along with relatively large amplitude EEG signals that follow the change in blood volume (Vanhataloa et al., 2003) (Fig. 5A). Tilting the head up or down (Fig. 5A), as well as compression of the jugular vein, give similar results (Vanhataloa et al., 2003). Complementary experiments that involve vasodilation support the hypothesis that slow potentials are generated by a change in volume of the blood. In particular, inhalation of carbon dioxide causes vasodilation on the time scale of minutes (Besson et al., 1970; Ngai and Winn, 1996) and leads to concurrent changes in the EEG signal in the < 1 Hz frequency range (Voipio et al., 2003).

The gold standard in these neurovascular studies is to record slow changes in the ECoG that are induced by vasodynamics concurrent with the electrical activity of nearby neurons. Such studies were performed with cats, in which the CO_2 content of the inhalation gas could be altered to induce vasodilation (Nita et al., 2004). Consistent with a vascular, but not with a neuronal origin of ultra-slow electrical signals, simultaneous intracellular recordings from neurons (Fig. 5B) and astrocytes show that the ultra-slow ECoG signals are reflected in neither the neuronal nor astrocyte membrane potential (Nita et al., 2004). Further, extracellular measurements as a function of depth in cortex failed to find a reversal of the

polarity of the ultra-slow signals with cortical depth, inconsistent with a synaptic origin of these potentials (Nita et al., 2004). In toto, the data refute the notion that ultra-slow neuronal signals are present in ultra-slow brain-wide ECoG signals, as opposed to the modulatory signal of the high frequency γ-band carrier seen in the ECoG.

Are there other neuronal origins of ultra-slow electrical activity? Intracellular neuronal currents with variation in the ~ 1 Hz range have been described (Steriade et al., 1993), but there are no reports of slower ionotropic currents with the exception of nicotinic acetylcholine receptors that contain the α7 and β2 receptor subunits. These subunits may play an important role in the generation of ultra-slow fluctuations in the spike rates of neurons in frontal cortex (Koukouli et al., 2016). Other ion channels show depolarization-induced changes in recovery times that last up to hundreds of seconds (Toib et al., 1998) and spontaneous synaptic release shows correlations over a multiplicity of long time-scales (Lowen et al., 1997). While currents that rely on reaction-diffusion kinetics and concentration dependent rates can be quite slow, they are not a priori oscillatory in nature.

Targeted neuromodulatory input to cortex.

There is evidence that slow signals from cholinergic modulatory centers provide brain-wide modulation of the γ-rhythm (Turch et al., 2018). The composite evidence also suggests that cholinergic signaling activates the M5 metabotropic pathway (Yamada et al., 2001) in penetrating arterioles (Adachi et al., 1992; Hotta et al., 2013; Sato et al., 2001; Vaucher and Hamel, 1995). Several studies have shown that projections from the basal forebrain, which contains a prominent cholinergic center, are targeted to specific brain regions (Kim et al., 2016a; Saper, 1984; Wu et al., 2014; Zaborszky et al., 2015). In particular, cholinergic targeting is specific at least down to the level of primary sensory areas (Kim et al., 2016a), consistent with the murine projectome of the basal forebrain (Li et al., 2018). Some cholinergic neurons could co-target functionally related areas (Li et al., 2018), though finer-scale organization, like retinotopy, may not be present (Huppé-Gourgues et al., 2018). The inputs to basal forebrain neurons also show a targeted input from different brain regions (Gielow and Zaborszky, 2017).

The neuromodulator noradrenaline, released by projections from the locus coeruleus, also functions to change brain-wide behavior. Chemogenetic activation of the locus coeruleus leads to an increase in the functional connectivity, as determined from the pair-wise cross-correlations among signals from different brain regions (Zerbi et al., 2019). However, unlike the case for basal forebrain input, the projections from locus coeruleus appear to be cortex-wide and diffuse, with no evidence for regional projections (Kim et al., 2016a). Of interest, noradrenaline release leads to global activation as a function of the cognitive task (Cardoso et al., 2019).

We conclude that vasomotion could in principle phase-lock to slow variations in neuromodulation. Only cholinergic modulatory input has the regional specificity that suggests feasibility, yet even for this case there is no evidence for changes in modulation on the short, 2 mm correlation length scale seen in rodents (He et al., 2018; Mateo et al., 2017). Nor is there published evidence for even broad-band oscillations at the ~ 0.1 Hz range.

While we cannot dismiss neuromodulation as a candidate mechanism for locking vasomotion to neuronal activity, current evidence deems it untenable.

ULTRA-SLOW VARIATIONS IN γ-BAND POWER ENTRAINS VASOMOTION

The ability to measure electrophysiological quantities concurrent with vasodynamics is essential to decipher the biophysical basis of resting-state BOLD fMRI signals (Villringer et al., 2006). A plethora of past work has made progress with the use of mixed electrical and optical-based recording of neuronal activity concurrent with measures of blood flow, often both hemodynamics and vasodynamics, in monkeys (Goense et al., 2012; Goense and Logothetis, 2008; Logothetis et al., 2012; Logothetis et al., 2001; Schölvinck et al., 2010; Shmuel et al., 2006; Shmuel and Leopold, 2008), rat (Du et al., 2014; He et al., 2018; Schwalm et al., 2017; Thompson et al., 2014), and mouse (Anenberg et al., 2014; Lee et al., 2010; Ma et al., 2016; Mateo et al., 2017; Pan et al., 2015; Schulz et al., 2012; Vanni et al., 2017; Wang et al., 2018; Winder et al., 2017). While mice have the great advantage of genetic introduction of functional labels, this can also lead to complications when the insertion of transgenes disrupt the coding sequence of endogenous genes (Goodwin et al., 2019) or labels lead to seizure activity (Steinmetz et al., 2017).

The connection between vasomotor oscillations in pial arterioles and fluctuation in the envelope of the γ-band of the local field potential (LFP) from the superficial layers was established in mouse (Mateo et al., 2017). We first consider the temporal variation in the spectral power of the LFP in the upper layers of cortex in relation to changes in the diameter of the surface arterioles (Fig. 6A). The field potential shows epochs of enhanced activity across all frequency bands. The variations in power are greatest in γ-band and, although episodic, are broadly distributed with a periodicity near 0.1 Hz. Crucially, changes in the diameter of surface arterioles co-vary with the power in the γ-band (Fig. 6B). The timing of the fluctuations is such that the electrical activity leads that of the diameter by ~ 2 s both in this example (Fig. 6C) and as an average over all observations. These data are consistent with the hypothesis that ultra-slow fluctuations in electrical activity drive changes in arteriole diameter. While the latency between increases in neuronal activity and vasodilation is ~ 2 s, that between the increase in neural activity and the BOLD fMRI signal is slightly longer, i.e., ~ 3 s, as a result of a delay of the increased oxygenated blood reaching the veins (Mateo et al., 2017) (Fig. 1A).

To test if local neuronal activity is sufficient to entrain vasomotion, the neuronal activity in mice that expressed channelrhodopsin in layer 5b pyramidal neurons was driven by light whose intensity modulated by a 40 Hz γ-rhythm carrier frequency and a 0.1 Hz ultra-slow rhythmic envelope (Mateo et al., 2017). We observed that the envelope of the γ-band and the diameter of a nearby arteriole are phase-locked, with electrical activity leading vasodilation by the same ~ 2 s as observed under natural conditions (Fig. 6C). These data confirm that ultra-slow modulation of high-frequency neuronal activity can entrain vasomotion.

The possibility that variations in arteriole diameter drive electrical activity was addressed through the use of mice that express halorhodopsin in arteriole smooth muscle (Mateo et al., 2017). Illumination of an arteriole with activating laser light leads to an ~ 0.2-times dilation,

similar to the value seen during vasomotion (Drew et al., 2011). Crucially, driving dilation of the smooth muscle fails to lead to a change in the LFP and a large drop in the spectral coherence between the vessel diameter and the driven envelope of the electrical activity. These data support the interpretation that vasomotion does not drive aggregate neuronal activity.

While the interaction between neuronal activity and vasomotion was unidirectional, an in vitro study has demonstrated feedback from blood vessels onto neuronal output (Kim et al., 2016b). Following pressurization of parenchymal arterioles, the vessels develop myogenic tone. A shift in the level of tone by challenging the arterioles with a change to higher pressure increases constriction, while lower pressures led to dilate. Importantly, upon an increase in pressure to induce vasoconstriction, pyramidal neurons suppressed their activity, while pressure-evoked dilation led to an increase in pyramidal neuron activity. The relation of this homeostatic feedback mechanism to neurovascular coupling remains an open issue.

‘Fidgeting’ movements are a driver of ultra-slow signals.

A potential contributor to the ultra-slow fluctuations in γ-band power are small motor movements of the face and limbs that are referred to as “fidgeting” (Drew et al., 2019; Winder et al., 2017). Studies with humans and primates have shown that blinking (Bristow et al., 2005; Guipponi et al., 2015), swallowing (Birn et al., 1999; Hamdy et al., 1999) and small head motions (Yan et al., 2013) are accompanied by bilateral activation of motor and somatosensory areas of the brain. Fidgeting appear to be independent of external sensation, but rather is a consequence of nonvolitional neuronal events. Fidgeting occurs at the rate of several events per minute, enabling these events to drive ultra-slow signals (Huo et al., 2014; Kaminer et al., 2011; Lear et al., 1965). Fidgeting can take place in absence of stimulation (Stringer et al., 2019) or accompany a learned task in mice (Musall et al., 2019; Salkoff et al., 2019), even though it is irrelevant to the task per se. For example, pressing a bar is accompanied by movements of the face and forelimbs and protraction of the vibrissae. Of relevance to blood flow, the functional form of the coupling between neuronal activity and hemodynamic signals appears the same for dilations evoked by either fidgeting, sensory stimuli, or volition (Power et al., 2012; Winder et al., 2017) (Fig. 6D,F).

Fidgeting is activated by neuronal motor circuits and presumably drives reafferent or efferent inputs to somatosensory regions in cortex. Thus, in principle, fidgeting can drive vasodilation and entrain vasomotion. We obtained new data to characterize the relation of fidgeting to the entrainment of vasomotion in alert, head-fixed, wild type mice. Following past methods (Winder et al., 2017), we recorded vibrissa movement, body movement, and concurrent changes in the diameter of pial arterioles (Fig. 6D; experimental details in the legend). Epochs of spontaneous whisking and body motion are observed, the largest of which are clearly correlated with relatively large, transient vasodilation events. As an average over mice and vessels, we observe that the movement precedes the vasodilation by ~ 2 s for both whisking and whole body motion (Fig. 6E), similar to that for the γ-band power (Fig. 6C). Thus, fidgeting is a likely contributor to the source of ultra-slow neuronal activity, albeit this shifts the question to what neuronal or environmental source drives fidgeting.

We performed a quantitative assessment of the contribution of body movement to the neuronal entrainment of vasomotion across our existing data with head-fixed mice (Mateo et al., 2017) (Fig. 6A–C). Previously unpublished accelerometer records of the motion of the body of the mouse were used to determine the contribution of fidgeting to vasomotion (Fig. 6F; experimental details in the legend). As an average over mice and vessels, body motion leads to transient dilation of the pial arterioles that rises over an interval of 2 s, the same as that for stimulus driven changes in arteriole diameter (Fig. 1A). The movement related changes in diameter encompassed 0.27 of the significantly correlated changes between vessel diameter and the γ-band LFP (center Fig. 6F). Critically, fidgeting was correlated with the largest dilations (right Fig. 6F). In toto, fidgeting is a significant contributor to the neurological events that entrain vasomotion in mice.

We suggest that fidgeting is likely to play a role in the origin of human resting-state BOLD fMRI signals as well (Drew et al., 2019). The punctate nature of fidgeting events is consistent with the punctate, albeit loosely rhythmic nature of resting-state activity in humans (Liu et al., 2018; Liu and Duyn, 2013; Petridou et al., 2013) and fidgeting behaviors often involve bilateral actions (Drew et al., 2019), consistent with the bilateral nature of spontaneous activations (Fig. 2D). Fidgeting behaviors are likely to be associated with BOLD fMRI signals in regions outside sensory and motor areas of the brain, including areas activated by cognitive tasks (Drew et al., 2019). For example, swallowing activates the insula (Martin et al., 2001) and licking (Nakano et al., 2013) and head motion (Bright and Murphy, 2015) activate multiple brain regions. It is an open issue if the sensorimotor processing that is associated with fine-scale self-motion is part of the ideation captured by resting-state BOLD fMRI. Nonetheless, experimental designs exist that can flag and censor epochs of even modest self-motion in human subjects (Power et al., 2012; Siegel et al., 2014).

Transitions among behavioral states may drive ultra-slow signals.

A seemingly high proportion of the resting-state BOLD fMRI studies in animals and humans did not closely monitor behavior or arousal. Thus, a wide variety of behavioral states may be sampled and averaged together. Head-fixed mice will sleep with their eyes open (Yüzgeç et al., 2018), so careful physiological monitoring of body motion, pupil motion, and pupil size is needed to ensure that the sleep-state vasodynamics (Fultz et al., 2019; Horovitz et al., 2009) do not contaminate resting-state measurements. Post hoc examination of human connectome data has indicated many if not most subjects fall asleep during the scanning process (Tagliazucchi and Laufs, 2014). Sleep-to-wake transitions (Horovitz et al., 2009; Liu et al., 2018) may thus drive events that account for a substantial component of functional connectivity (Liu and Duyn, 2013; Petridou et al., 2013).

MECHANISMS FOR CORRELATED BILATERAL VASODYNAMICS

The dominant feature of resting-state connectivity is the bilateral symmetry across hemispheres (Fig. 2D). The details of bilateral coactivation can be explored via the coherence between changes in arteriole diameter for vessels in mirrored regions. In fact, precise, simultaneous measurements of vessel diameter show that arterioles in mirrored regions oscillate in synchrony with near unity coherence (Mateo et al., 2017) (Fig. 3C). The

coherence is severely reduced in acallosal mice (Mateo et al., 2017), consistent with the finding that bilateral neuronal signaling is similarly reduced in acallosal mice (Mohajerani et al., 2010). Yet, as noted previously, the evidence for mirrored activation in acallosal human subjects is equivocal.

Vascular geometry that enhances bilateral symmetry.

While the origin of symmetry in resting-state connectivity is typically attributed to interhemispheric projections, there are other systemic vascular contributors. Fluctuations in the inflow of blood at the level of the left and right carotids are strongly coherent at 0.01 - 0.3 Hz, i.e., the range of vasomotor frequencies in awake rats (Revel et al., 2012). Arterial blood oxygenation also fluctuates with fluctuations in respiration rate and with the respiratory cycle (Zhang et al., 2019). These lead to delayed fluctuations in the global BOLD fMRI signal throughout the brain and into the sagittal sinus (Tong et al., 2019). Unfortunately, the fluctuations from the carotid supply tend to dephase as blood travels with different transit times through the brain. Thus, fluctuations in inflow and oxygenation cannot be completely removed by regression of a brain-wide signal (Tong et al., 2015). A further complication occurs since vasomotion will change the transit times. Thus, measures of blood oxygenation can be systematically biased if they occur at locations with different transit times, as opposed to mirrored brain regions. For this reason, recent reports of small shifts in the timing of BOLD fMRI signals in humans (Mitra et al., 2015) could be the result of small changes in the perfusion times or oxygenation of blood to different regions of the brain. As a clinical matter, this effect can highlight perfusion deficits after stroke (Lv et al., 2012) and may explain how low-grade brain tumors show coherent oscillations in the BOLD fMRI with their putatively healthy contralateral brain regions (Gupta et al., 2018).

Bilaterally-synchronized modulatory inputs can drive bilateral oscillations.

There are direct, cholinergic cross-hemispheric connections between the basal forebrain in the two hemispheres (Carnes et al., 1990; Semba et al., 1988). These connections should not be affected in acallosal animals, thus preserving common input to mirrored, transhemispheric cortical regions.

Activation of the rostral ventral lateral medulla (RVLM), a brainstem nucleus that sits on the ventral surface of the brain below the breathing center (Golanov et al., 1994) leads to an increase in cortical blood flow. This nucleus receives input from neighboring breathing centers (Dempsey et al., 2017) and will increase blood flow in response to a decrease in atmospheric pO_2 (Golanov and Reis, 1996). The RVLM contains primarily noradrenergic neurons (Abbott et al., 2012). The limited anatomical studies published to date have not identified direct nor complete indirect projections from RVLM to the cortex (Card et al., 2006). Nonetheless, in one likely pathway, the RVLM projects to the medullary cerebral vasodilator area in brainstem, then projects to the subthalamic cerebral vasodilator area in the diencephalon, which incorporates zona incerta and the Fields of Forel, and finally projects to deep layers of cortex (Golanov et al., 2001; Ilcha and Golanov, 2004). The specifics of the drive to cortical blood vessels is an open issue.

TECHNICAL SOURCES OF ULTRA-SLOW NOISE CONTRIBUTIONS IN fMRI

As a means to reduce voluntary motion of the head, contemporary rodent resting-state fMRI studies have been primarily performed on anesthetized head-fixed but free-breathing animals (Biswal and Kannurpatti, 2009; Williams et al., 2010; Zhao et al., 2008). However, cardiac- and respiratory-based artifacts in rodent resting-state BOLD and CBV fMRI remain to be carefully identified and removed from the data. These difficulties stand in contrast to the significant efforts made for the human BOLD fMRI studies (Birn et al., 2006; Dagli et al., 1999; Glover and Li, 2000; Hu et al., 1995; Shmueli et al., 2007; Wise et al., 2004). The adoption of signal processing methods developed for human studies (Caballero-Gaudes and Reynolds, 2017; Murphy et al., 2013) will be crucial to reduce the interference of cardiorespiratory artifacts with the spatiotemporal patterns of the resting-state fMRI signals in animals (Abreu et al., 2017; Biswal et al., 1996; Bright and Murphy, 2017; Feinberg and Setsompop, 2013; Kiviniemi et al., 2005).

Respiration-induced "B_0 offset" motion.

Magnetic resonance image acquisition relies on Larmor frequency-based spatial encoding through the sequence-specific magnetic field gradients across a subject. The homogeneity of the constant magnetic field, designated B_0, determines the quality of magnetic resonance images (Durand et al., 2001). However, the subject inside the magnetic resonance scanner can continually disturb the homogeneity of the B_0 field by movement of their body (Biswal et al., 1996; Frank et al., 2001; Lowe et al., 1998; Van de Moortele et al., 2002). This includes fidgeting (Fig. 6D) as well as breathing and other physiological motions. In practice, breathing leads to an expanding and contracting B_0 field near the brain (Fig. 7A). Thus, artifacts in BOLD MRI can originate from parts of the body that are far away from the field of view in the brain (Fig. 7B).

Methods to compensate for the time-dependent B_0 field distortions are known (Raj et al., 2000; van Gelderen et al., 2007). Yet, in contrast to studies on human subjects, the higher magnetic fields used for animal BOLD and CBV fMRI studies will exaggerate the effects of physiological contributions to an inhomogeneous B_0 field. In addition, both arteriole CO_2 (Wise et al., 2004) and respiratory volume changes (Birn et al., 2006) can cause variations in the resting-state BOLD fMRI signals that lead to falsely interpreted signals.

Aliasing of physiological rhythms.

Rats have an approximately 5 - 7 Hz cardiac frequency and approximately 1 - 2 Hz respiration rates under anesthesia. The conventional echo-planar imaging protocol with rodents involves a 1 - 2 s period of repetition (TR) or equivalently a sampling rate, denoted f_s, of $f_s = 1/\mathrm{TR} = 0.5 - 1.0$ Hz. The low rate of sampling compared to physiological processes that distort the fMRI signal will cause aliasing of both cardiac and respiratory contributions down to frequencies that may also be erroneously associated with resting-state dynamics. This is well described for human resting-state fMRI studies (Biswal et al., 1996; Dagli et al., 1999; De Luca et al., 2006; Frank et al., 2001; Lowe et al., 1998) and is seen in rat as well (Pais-Roldan et al., 2018). For example, when the sampling rate is $f_s = 0.8$ Hz and the spontaneous breathing rate of an anesthetized rat is $f_B = 1.0 \pm 0.1$ Hz, the signal is

aliased to $f_B - f_s = 0.2 \pm 0.1$ Hz. This is illustrated by measuring breathing at $f_s >> f_B$ and observing the aliased rate that is seen when the data is down-sampled to $f_s = 0.8$ Hz (Fig. 7C). Aliasing is observed in the fMRI signal of both brain and a phantom above the head of the animal when the sampling rate is $f_s = 0.8$ Hz (Fig. 7C). This illustrates the combined effect of distortion of the B_0 field and aliasing to form a false image of a resting-sate signal (Fig. 7D).

Fast fMRI methods clearly will avoid aliasing of both the cardiac and respiratory contributions to the fMRI signals from rodents (Williams et al., 2010; Yu et al., 2014). A similar fast sampling strategy has been well implemented to remove the physiological noise for fMRI measurements from human brains (Agrawal et al., 2020). However, it is much more difficult to avoid the higher frequency cardiac-specific aliasing artifacts, especially for awake rodent fMRI (Desai et al., 2011; Ferenczi et al., 2016; Liang et al., 2015). Further, cardiac and respiratory cycles can fluctuate individually and in a coupled manner at frequencies close to the ~ 0.1 Hz frequency range for ultra-slow signals. These fluctuations can serve as additional, confounding sources for resting-state BOLD fMRI studies (Shmueli et al., 2007).

CONCLUSIONS

Motivated by a desire to understand the biophysical basis of resting-state fMRI (Fig. 2), we have reviewed data on the relation of spontaneous changes in blood flow and blood oxygenation in the brain to changes in the underlying neuronal activity (Fig. 8A). Ultra-slow vasomotor oscillations occur in the smooth muscle cells that encircle brain arterioles and lead to rhythmic changes in the diameter of arterioles within a frequency band near 0.1 Hz (Fig. 3). Further, collective neuronal dynamics in the forebrain lead to the generation of high frequency γ-band oscillations whose amplitude is modulated at the ultra-slow rate of ~ 0.1 Hz. (Fig. 6B). These ultra-slow neuronal oscillations will entrain the arteriole oscillations to link brain vasodynamics with nonvolitional neuronal activity (Figs. 6A–C). The entrainment is statistically significant (Fig. 6), even though the vasculature also responds to common, cortex-wide inputs and homeostatic physiological inputs. The entrainment of vasomotion by neuronal spiking provides a means for arterioles in regions of the brain that are separated yet connected through callosal projections to have synchronous vasomotor activity (Fig. 3C). Within the technological framework of fMRI, vasomotor activity can be measured through changes in arteriole volume, i.e., CBV fMRI, or changes in blood oxygenation secondary to changes in diameter, i.e., BOLD fMRI. The flow diagram of Figure 8A formalizes this description.

Significance of the ultra-slow coupling.

Functional MRI allows one to ‘decode’ the neural activity in the brain to the extent that neural activity is represented by BOLD signals (Kay et al., 2008). A key issue is how well hemodynamic signals report neural activity. In Supplemental Table 1 we list the correlation coefficient R^2, the so-called “variance explained”, between neural activity and either the BOLD or CBV fMRI or equivalent optical signal; Supplemental Text Box 1 relates R^2 to the spectral coherence, $C(f)$. In all of these studies there was a highly significant correlation

between the hemodynamic response and neural activity. This means that resting-state BOLD fMRI signal or equivalent are, to varying extents, driven by neural activity. Yet the value of R^2 is universally less than 0.5 and typically around 0.1 (Schölvinck et al., 2010; Shmuel and Leopold, 2008). This means that only 0.1 to 0.5 of the hemodynamic signal is related to neural activity. A value of $R^2 = 0.5$ between γ-band neuronal activity and the simultaneously recorded BOLD fMRI signal occurs for visual stimulus-evoked activity in the un-anesthetized primate (Goense and Logothetis, 2008). Given the strong drive of visual stimuli, this suggest that the value $R^2 = 0.5$ seen in rest-state measurement is likely to be is an upper bound. If we further consider that fidgeting occurs ~ 0.3 of the time, as an upper bound we expect that at the most 0.5 x 0.7 ~ 0.4 of the resting-state BOLD fMRI signal is related to internally driven brain dynamics. Thus resting-state BOLD fMRI, as currently practiced, provides unique capabilities to infer connectivity in the human brain, yet is a technique with an inherently low signal-to-noise ratio.

The role of vasomotion.

What is the normal, physiological purpose served by the ultra-slow vasomotor oscillations of brain arterioles? Recent work points to the necessity of vasomotion for the clearance of large solutes (van Veluw et al., 2020), principally through the paravascular space between the smooth muscle and endothelial cells (Cserr and Ostrach, 1974; Rennels et al., 1985). These solutes include β-amyloid (Iliff et al., 2012). To the extent that vasomotion is entrained by the envelope of the γ-band power (Mateo et al., 2017) (Fig. 6), it is of interest whether increases in γ-power in the brain through sensory stimulation also increases the clearance of β-amyloid (Iaccarino et al.). The ability of vasomotion to drive solutes must depend on a mechanism to set the direction of flow, such as peristaltic motion (Aldea et al., 2019) or yet-to-be discovered valves in the paravascular space (Mathiisen et al., 2010).

Next steps.

The nature of the local neuronal circuitry that generates ultra-slow signals and modulates the γ-rhythm remains an open issue. In particular, the exact frequency of ultra-slow signals varies across the brain with millimeters to centimeters of coherence (Mitra et al., 1997; Vanni et al., 2017) (Fig. 2B). Such spatially restricted modulation could be accomplished by even small changes in the activation of currents in individual cells that contribute to generate the γ-rhythm (Kopell and LeMasson, 1994). In this way, the ultra-slow signals are purely modulatory (Fig. 4) and the ECoG will not contain ultra-slow signals (Fig. 5).

Recent work describes a fast mechanism to transform subsurface microvasculature signaling into changes in arteriole diameter (Longden et al., 2017) (Fig. 1C). Yet the nature of electrical signaling across the lattice of pial surface vasculature remains to be solved (Hillman, 2014). At a phenomenological level, the pial arteriole oscillators form two sets of interactions (Fig. 8B). On the one hand, each arteriole is directly connected with four neighboring oscillators (Blinder et al., 2010) via gap junctions between endothelial cells (Fig. 1C); this connectivity acts to frequency lock vasomotion across all vessels across the surface (Sakaguchi et al., 1988; Strogatz and Mirolla, 1988). On the other hand, underlying neurons can drive the local pial vessels at different frequencies; this should break the coherence of vessels across the cortical mantle so that the vessels parcellate into regions

with different vasomotor center frequencies (Fig. 8B). BOLD fMRI data from humans supports such a parcellation on the scale of tens of millimeters (Fig. 1B). In fact, such parcellation has been used to segment different regions in cortex (Fox et al., 2005; Glasser et al., 2016). Animal models, together with large-field, high precision optical imaging (Sofroniew et al., 2016; Tsai et al., 2015), should allow us to assess the phenomenology and the biophysics for this parcellation.

A more accurate and high resolution measure of functional connectivity may be obtained through measurements of CBV rather than BOLD fMRI (He et al., 2018). When the spatial resolution of fMRI can distinguish individual vessels that penetrate the cortex of the rat brain (Moon et al., 2013; Poplawsky et al., 2019; Yu et al., 2012), the BOLD fMRI signal is located mainly at venule voxels while the CBV fMRI signal is detected primarily at arteriole voxels (He et al., 2018; Yu et al., 2016). Thus the single-vessel fMRI method will enable detection of the spatial correlation patterns of the resting-state signal with vascular specificity, as seen optically in restricted regions (Mateo et al., 2017) (Fig. 3C). From a technical perspective, the spatial localization of single-vessel fMRI decouples the resting-state signal from respiration-induced B_0-related motion artifacts (Fig. 7). The ability to resolve individual penetrating vessels with CBV fMRI provides a critical platform to explore the ultra-slow oscillatory patterns of vasodynamics across the brain. This is particularly important for understanding how pair-wise interactions among different brain regions may lead to the great multitude of “default networks” of rodent (Chan et al., 2015; Ma et al., 2016; Mohajerani et al., 2013; Mohajerani et al., 2010) and human (Greicius et al., 2003; Raichle et al., 2001; Sporns et al., 2005) brain activity.

Finally, as a practical matter, experimenters should monitor behavior and arousal state as much as possible to differentiate between activity generated during spontaneous movements, sleep, and activity generated during true “rest” (Drew et al., 2019). Monitoring of behavioral state has become de rigueur in systems neuroscience experiments using awake rodents and primates (Egnor and Branson, 2016; Whishaw and IQ Whishaw, 2014), makes use of standard equipment for studies with rodents (Kurnikova et al., 2017; Mathis et al., 2018; Reimer et al., 2014), and should be adopted by the human fMRI community as well. Thus, it may be possible to use behavioral event markers to segregate resting-state epochs with fidgeting from those without these movements and presumably increase the sensitivity to purely intrinsically driven brain-wide changes in BOLD or CBV fMRI signals.

Supplementary Material

Refer to Web version on PubMed Central for supplementary material.

Acknowledgements

We thank David Boas, Thomas Broggini, Jean-Pierre Changeux, Karishma Chhabria, Anna Devor, Jessica Filosa, Partha Mitra, Mark Nelson, Jonathan Polimeni, Bruce Rosen, and Massimo Vergassola for valuable discussions. We thank Beth Friedman for comments on drafts of this manuscript. This work was supported by grants EB0217003, MH114224, and NS078168 to PJD, MH111438 and NS097265 to DK, NS113278 to XY, and the Max Planck Society.

References

Aalkjær C, Boedtkjer D, and Matchkov V (2011). Vasomotion – what is currently thought? Acta Physiologiae 202, 253–269.

Aalkjaer C, and Nilsson H (2005). Vasomotion: Cellular background for the oscillator and for the synchronization of smooth muscle cells. British Journal of Pharmacology 144, 605–616. [PubMed: 15678091]

Abbott SB, Kanbar R, Bochorishvili G, Coates MB, Stornetta RL, and Guyenet PG (2012). C1 neurons excite locus coeruleus and A5 noradrenergic neurons along with sympathetic outflow in rats. Journal of Physiology 590, 2897–2915.

Abreu R, Nunes S, Leal A, and Figueiredo P (2017). Physiological noise correction using ECG-derived respiratory signals for enhanced mapping of spontaneous neuronal activity with simultaneous EEG-fMRI. Neuroimage 154, 115–127. [PubMed: 27530551]

Adachi T, Baramidze DG, and Sato A (1992). Stimulation of the nucleus basalis of Meynert increases cortical cerebral blood flow without influencing diameter of the pial artery in rats. Neuroscience Letters 143, 173–176. [PubMed: 1436664]

Agrawal U, Brown EN, and Lewis LD (2020). Model-based physiological noise removal in fast fMRI. Neuroimage 205, e116231.

Ahrens KF, Levine H, Suhl H, and Kleinfeld D (2002). Spectral mixing of rhythmic neuronal signals in sensory cortex. Proceedings of the National Academy of Sciences USA 99, 15176–15181.

Aldea R, Weller RO, Wilcock DM, Carare RO, and Richardson G (2019). Cerebrovascular smooth muscle cells as the drivers of intramural periarterial drainage of the brain. Frontiers in Aging Neuroscience 11, e1.

Anenberg E, Arstikaitis P, Niitsu Y, Harrison TC, Boyd JD, Hilton BJ, Tetzlaff W, and Murphy TH (2014). Ministrokes in channelrhodopsin-2 transgenic mice reveal widespread deficits in motor output despite maintenance of cortical neuronal excitability. Journal of Neuroscience 34, 1094–1104. [PubMed: 24453302]

Attwell D, Buchan AM, Charpak S, Lauritzen M, MacVicar BA, and Newman EA (2010). Glial and neuronal control of brain blood flow. Nature 468, 232–243. [PubMed: 21068832]

Bandettini PA, Wong EC, Hinks RS, Tikofsky RS, and Hyde JS (1992). Time course EPI of human brain function during task activation. Magnetic Resonance in Medicine 25, 390–398. [PubMed: 1614324]

Barson D, Hamodi AS, Shen X, Lur G, Constable RT, Cardin JA, Crair MC, and Higley MJ (2019). Simultaneous mesoscopic and two-photon imaging of neuronal activity in cortical circuits. Nature Methods 16, 1–7. [PubMed: 30573832]

Belliveau JW, Kennedy DN, McKinstry RC, Buchbinder BR, Weisskoff RM, Cohen MS, Vevea JM, Brady TJ, and Rosen BR (1991). Functional mapping of the human cortex using magnetic resonance imaging. Science 254, 716–719. [PubMed: 1948051]

Besson JM, Woody CD, Aleonard P, Thompson HK, Albe-Fessard D, and Marshall WH (1970). Correlations of brain d-c shifts with changes in cerebral blood flow. American Journal of Physiology 218, 284–291.

Birn RM, Bandettini PA, Cox RW, and Shaker R (1999). Event-related fMRI of tasks involving brief motion. Human Brain Imaging 7, 106–114.

Birn RM, Diamond JB, Smith MA, and Bandettini PA (2006). Separating respiratory-variation-related neuronal-activity-related fluctuations in fluctuations from fMRI. Neuroimage 31, 1536–1548. [PubMed: 16632379]

Biswal B, DeYoe EA, and Hyde JS (1996). Reduction of physiological fluctuations in fMRI using digital filters. Magnetic resonance in Medicine 35, 107–113. [PubMed: 8771028]

Biswal B, Yetkin FZ, Haughton VM, and Hyde JS (1995). Functional connectivity in the motor cortex of resting human brain using echo-planar MRI. Magnetic Resonance in Medicine 34, 537–541. [PubMed: 8524021]

Biswal BB, and Kannurpatti SS, eds. (2009). Resting-state functional connectivity in animal models: Modulations by exsanguination (Springer Protocols).

Biswal BB, Maarten Mennes M, Zuo X-N, Gohel S, Kelly C, Smith SM, Beckmann CF, Adelstein JS, Buckner RL, Stan Colcombe S, et al. (2010). Toward discovery science of human brain function. Proceedings of the National Academy of Sciances USA 10, 4734–4739.

Black HS (1953). Modulation Theory (New York: Van Nostrand).

Blinder P, Shih AY, Rafie CA, and Kleinfeld D (2010). Topological basis for the robust distribution of blood to rodent neocortex. Proceedings of the National Academy of Sciences USA 107, 12670–12675.

Bohland JW, Wu C, Barbas H, Bokil H, Bota M, Breiter HC, Cline HT, Doyle JC, Freed PJ, Greenspan RJ, et al. (2009). A proposal for a coordinated effort for the determination of brainwide neuroanatomical connectivity in model organisms at a mesoscopic scale. Public Library of Science: Computational Biology 5, e1000334. [PubMed: 19325892]

Branscomb LM (1995). Confessions of a Technophile (American Institute of Physics).

Bright MG, and Murphy K (2015). Is fMRI “noise” really noise? Resting state nuisance regressors remove variance with network structure. Neuroimage 114, 158–169. [PubMed: 25862264]

Bright MG, and Murphy K (2017). Cleaning up the fMRI time series: Mitigating noise with advanced acquisition and correction strategies. NeuroImage 154, 1–3. [PubMed: 28365420]

Bristow D, Frith C, and Rees G (2005). Two distinct neural effects of blinking on human visual processing. Neuroimage 27, 136–145. [PubMed: 15893941]

Buxton RB (2001). The elusive initial dip. Neuroimage 13, 953–958. [PubMed: 11352601]

Caballero-Gaudes C, and Reynolds RC (2017). Methods for cleaning the BOLD fMRI signal. NeuroImage 154, 128–149. [PubMed: 27956209]

Caesar K, Akgören N, Mathiesen C, and Lauritzen M (1999). Modification of activitydependent increases in cerebellar blood flow by extracellular potassium in anaesthetized rats. Journal of Physiology 520, 281–292.

Card JP, Sved JC, Craig B, Raizada M, Vazquez J, and Sved AF (2006). Efferent projections of rat rostroventrolateral medulla C1 catecholamine neurons: Implications for the central control of cardiovascular regulation. Journal of Comparative Neurology 499, 840–859.

Cardin JA, Carlén M, Meletis K, Knoblich U, Zhang F, Deisseroth K, Tsai LH, and Moore CI (2009). Driving fast-spiking cells induces gamma rhythm and controls sensory responses. Nature 459, 663–667. [PubMed: 19396156]

Cardoso MMB, Lima B, Sirotin YB, and Das A (2019). Task-related hemodynamic responses are modulated by reward and task engagement. Public Library of Science: Biology 17, e3000080. [PubMed: 31002659]

Carnes KM, Fuller TA, and Price JL (1990). Sources of presumptive glutamatergic/aspartatergic afferents to the magnocellular basal forebrain in the rat. Journal of Comparative Neurology 302, 824–852.

Cauli B, and Hamel E (2010). Revisiting the role of neurons in neurovascular coupling. Frontiers of Neuroenergetics 9, e00009.

Chan AW, Mohajerani MH, LeDue JW, Wang YT, and Murphy TH (2015). Mesoscale infraslow spontaneous membrane potential fluctuations recapitulate high-frequency activity cortical motifs. Nature Communications 6, 7738.

Cserr HF, and Ostrach LH (1974). Bulk flow of interstitial fluid after intracranial injection of blue dextran 2000. Experimental Neurology 45, 50–60. [PubMed: 4137563]

Dacey RG Jr, and Duling BR (1984). Effect of norepinephrine on penetrating arterioles of rat cerebral cortex. Americal Journal of Physiology - Heart and Circulatory Physiology 246, 380–385.

Dagli MS, Ingeholm JE, and Haxby JV (1999). Localization of cardiac-induced signal change in fMRI. Neuroimage 9, 407–415. [PubMed: 10191169]

De Luca M, Beckmann CF, De Stefano N, and Matthews PM (2006). fMRI resting state networks define distinct modes of long-distance interactions in the human brain. Neuroimage 29, 1359–1367. [PubMed: 16260155]

De Luca M, Smith S, De Stefano N, Federico A, and Matthews PM (2005). Blood oxygenation level dependent contrast resting state networks are relevant to functional activity in the neocortical sensorimotor system. Experimental Brain Research 167, 587–594. [PubMed: 16284751]

Dempsey B, Le S, A. T, Bokiniec P, Ramadas R, Bjaalie JG, Menuet C, Neve R, Allen AM, Goodchild AK., et al. (2017). Mapping and analysis of the connectome of sympathetic premotor neurons in the rostral ventrolateral medulla of the rat using a volumetric brain atlas. Frontiers in Neural Circuits 11, e9.

Desai M, Kahn I, Knoblich U, Bernstein J, Atallah H, Yang A, Kopell N, Buckner RL, Graybiel AM, Moore CI, et al. (2011). Mapping brain networks in awake mice using combined optical neural control and fMRI. Journal of Neurophysiology 105, 1393–1405. [PubMed: 21160013]

Drew PJ, Duyn JH, Golanov E, and Kleinfeld D (2008). Finding coherence in spontaneous oscillations. Nature Neuroscience 11, 991–993. [PubMed: 18725901]

Drew PJ, Shih AY, Driscoll JD, Knutsen PM, Davalos D, Blinder P, Akassoglou K, Tsai PS, and Kleinfeld D (2010). Chronic optical access through a polished and reinforced thinned skull. Nature Methods 7, 981–984. [PubMed: 20966916]

Drew PJ, Shih AY, and Kleinfeld D (2011). Fluctuating and sensory-induced vasodynamics in rodent cortex extends arteriole capacity. Proceedings of the National Academy of Sciences USA 108, 8473–8478.

Drew PJ, Winder AT, and Zhang Q (2019). Twitches, blinks, and fidgets: Important generators of ongoing neural activity. The Neuroscientist 25, 298–313. [PubMed: 30311838]

Du C, Volkow ND, Koretsky AP, and Pan Y (2014). Low-frequency calcium oscillations accompany deoxyhemoglobin oscillations in rat somatosensory cortex. Proceedings of the National Academy of Sciences USA 111, 4677–4686.

Durand E, van de Moortele PF, and Pachot-Clouard M (2001). Artifact due to B-o fluctuations in fMRI: Correction using the k-space central line. Magnetic Resonance in Medicine 48, 198–201.

Egnor SER, and Branson K (2016). Computational analysis of behavior. Annual Review of Neuroscience 39, 217–236.

Engel A, Konig P, Kreiter AK, and Singer W (1991). Interhemispheric synchronization of oscillatory neuronal responses in cat visual cortex. Science 252, 1177–1179. [PubMed: 2031188]

Feinberg DA, and Setsompop K (2013). Ultra-fast MRI of the human brain with simultaneous multi-slice imaging. Journal of Magnetic Resonance 229, 90–100. [PubMed: 23473893]

Ferenczi EA, Zalocusky KA, Liston C, Grosenick L, Warden MR, Amatya D, Katovich K, Mehta H, Patenaude B, Ramakrishnan C, et al. (2016). Prefrontal cortical regulation of brainwide circuit dynamics and reward-related behavior. Science 351, e9698.

Ferezou I, Haiss F, Gentet LJ, Aronoff R, Weber B, and Petersen CCH (2007). Spatiotemporal dynamics of cortical sensorimotor integration in behaving mice. Neuron 56, 907–923. [PubMed: 18054865]

Filosa JA, Bonev AD, Straub SV, Meredith AL, Wilkerson MK, Aldrich R, and Nelson MT (2006). Local potassium signaling couples neuronal activity to vasodilation in the brain. Nature Neuroscience 9, 1397–1403. [PubMed: 17013381]

Fox MD, and Raichle ME (2007). Spontaneous fluctuations in brain activity observed with functional magnetic resonance imaging. Nature Reviews of Neuroscience 8, 700–711. [PubMed: 17704812]

Fox MD, Snyder AZ, Vincent JL, Corbetta M, Van Essen DC, and Raichle ME (2005). The human brain is intrinsically organized into dynamic, anticorrelated functional networks. Proceedings of the National Academy of Sciences USA 102, 9673–9678.

Fox PT, and Lancaster JL (2002). Mapping context and content: The BrainMap mode. Nature Reviews of Neuroscience 3, 319–321.

Frank LR, Buxton RB, and Wong EC (2001). Estimation of respiration-induced noise fluctuations from undersampled multislice fMRI data. Magnetic Resonance in Medicine 45, 635–644. [PubMed: 11283992]

Fultz NE, Bonmassar G, Setsompop K, Stickgold RA, Rosen BR, olimeni JR, and Lewis LD (2019). Coupled electrophysiological, hemodynamic, and cerebrospinal fluid oscillations in human sleep. Science 366, 628–631. [PubMed: 31672896]

Gao YR, Ma Y, Zhang Q, Winder AT, Liang Z, Antinori L, Drew PJ, and Zhang N (2017). Time to wake up: Studying neurovascular coupling and brain-wide circuit function in the un-anesthetized animal. Neuroimage 153, 382–398. [PubMed: 27908788]

Gielow MR, and Zaborszky L (2017). The input-output relationship of the cholinergic basal forebrain. Cell Reports 18, 1817–1830. [PubMed: 28199851]

Glasser MF, Coalson TS, Robinson EC, D. HC, Harwell J, Yacoub E, Ugurbil K, , Andersson J, Beckmann CF, Jenkinson M, et al. (2016). A multi-modal parcellation of human cerebral cortex. Nature 536, 171–178. [PubMed: 27437579]

Glover GH, and Li TQ (2000). Image-based method for retrospective correction of physiological motion effects in fMRI: RETROICOR. Magnetic Resonance in Medicine 44, 162–167. [PubMed: 10893535]

Goense J, Merkle H, Nikos K, and Logothetis NK (2012). High-resolution fMRI reveals laminar differences in neurovascular coupling between positive and negative BOLD responses. Neuron 76, 629–639. [PubMed: 23141073]

Goense JBM, and Logothetis NK (2008). Neurophysiology of the BOLD fMRI signal in awake monkeys. Current Biology 18, 631–640. [PubMed: 18439825]

Golanov EV, Christensen RC, and Reis DJ (2001). Neurons of a limited subthalamic area mediate elevations in cortical cerebral blood flow evoked by hypoxia and excitation of neurons of the rostral ventrolateral medulla. Journal of Neuroscience 21, 4032–4041. [PubMed: 11356890]

Golanov EV, and Reis DJ (1996). Contribution of oxygen-sensitive neurons of the rostral ventrolateral medulla to hypoxic cerebral vasodilatation in the rat. Journal of Physiology 495, 201–216.

Golanov EV, Yamamoto S, and Reis DJ (1994). Spontaneous waves of cerebral blood flow associated with a pattern of electrocortical activity. American Journal of Physiology - Regulatory, Integrative and Comparative Physiology 266, 204–214.

Goodwin LO, Splinter E, Davis TL, Urban R, He H, Braun RE, Chesler EJ, Kumar V, van Min M, Ndukum J, et al. (2019). Large-scale discovery of mouse transgenic integration sites reveals frequent structural variation and insertional mutagenesis. Genome Research 29, 494–505. [PubMed: 30659012]

Gozzi A, and Schwarz AJ (2016). Large-scale functional connectivity networks in the rodent brain. NeuroImage 127, 496–509. [PubMed: 26706448]

Greicius MD, Krasnow B, and Reiss AL (2003). Functional connectivity in the resting brain: A network analysis of the default mode hypothesis. Proceedings of the National Academy of Sciences USA 100, 253–258.

Greicius MD, Supekar K, Menon V, and Dougherty RF (2009). Resting-state functional connectivity reflects structural connectivity in the default mode network. Cerebral Cortex 19, 71–78.

Grinvald A, Frostig RD, Lieke E, and Hildesheim R (1988). Optical imaging of neuronal activity. Physiological Reviews 68, 1285–1366. [PubMed: 3054949]

Grinvald A, Frostig RD, Siegel RM, and Bartfeld E (1991). High-resolution optical imaging of functional brain architecture in the awake monkey. Proceedings of the National Academy of Sciences USA 88, 11559–11563.

Guipponi O, Odouard S, Pinede S, Wardak C, and Hamed SB (2015). fMRI cortical correlates of spontaneous eye blinks in the nonhuman primate. Cerebral Cortex 25, 2333–2345. [PubMed: 24654257]

Gupta L, Gupta RK, Postma AA, Sahoo P, Gupta PK, Patir R, Ahlawat S, Saha I, and Backes WH (2018). dvanced and amplified BOLD fluctuations in high-grade gliomas. Journal of Magnetic Resonance Imaging 47, 1616–1625. [PubMed: 28963852]

Haddock RE, and Hill CE (2005). Rhythmicity in arterial smooth muscle. Journal of Physiology 566, 645–656.

Hamdy S, Rothwell JC, Brooks DJ, Bailey D, Aziz Q, and Thompson DG (1999). Identification of the cerebral loci processing human swallowing with H215O PET activation. Journal of Neurophysiology 81, 1917–1926. [PubMed: 10200226]

Hansel D, Mato G, and Meunier C (1993). Phase dynamics for weakly coupled Hodgkin-Huxley neurons. Europhysics Letters 23, 367–372.

Harraz OF, Longden TA, Dabertrand F, Hill-Eubanks D, and Nelson MT (2018). Endothelial GqPCR activity controls capillary electrical signaling and brain blood flow through PIP2 depletion. Proceedings of the National Academy of Sciences USA 115, 3569–3577.

He BJ, and Raichle ME (2009). The fMRI signal, slow cortical potential and consciousness. Trends in Cognitive Sciences 13, 302–309. [PubMed: 19535283]

He Y, Wang M, Chen X, Pohmann R, Polimeni JR, Scheffler K, Rosen BR, Kleinfeld D, and Yu X (2018). Ultra-slow single-vessel BOLD and CBV-based fMRI spatiotemporal dynamics and their correlation with neuronal intracellular calcium signals. Neuron 97, 925–939. [PubMed: 29398359]

Held D, Fencl V, and R. PJ. (1964). Electrical properties of cerebralspina; fluid. Journal of Neurophysiology 27, 942–959. [PubMed: 14205013]

Hillman EM (2014). Coupling mechanism and significance of the BOLD signal: A status report. Annual Review of Neuroscience 37, 161–181.

Honey CJ, Sporns O, Cammoun L, Gigandet X, Thiran JP, Meuli R, and Hagmann P (2009). Predicting human resting-state functional connectivity from structural connectivity. Proceedings of the National Academy of Sciences USA 106, 2035–2040.

Horovitz SG, Fukunaga M, de Zwart JA, van Gelderen P, Fulton SC, Balkin TJ, and Duyn JH (2009). Low frequency BOLD fluctuations during resting wakefulness and light sleep: A simultaneous EEG-fMRI study. Human Brain Mapping 29, 671–682.

Hotta H, Masamoto K, Uchida S, Sekiguchi Y, Takuwa H, Kawaguchi H, Shigemoto K, Sudo R, Tanishita K, to H, et al. (2013). Layer-specific dilation of penetrating arteries induced by stimulation of the nucleus basalis of Meynert in the mouse frontal cortex. Journal of Cerebral Blood Flow & Metabolism 33, 1440–1447. [PubMed: 23756692]

Hu XP, Le TH, Parrish T, and Erhard P (1995). Retrospective estimation and correction of physiological fluctuation in functional MRI. Magnetic Resonance in Medicine 34, 201–212. [PubMed: 7476079]

Huber L, Handwerker DA, Jangraw DC, Chen G, Hall A, Stuber C, Gonzalez-Castillo J, Ivanov D, Marrett S, Guidi M, et al. (2017). High-resolution CBV-fMRI allows mapping of laminar activity and connectivity of cortical Input and output in human M1. Neuron 96, 1253–1263. [PubMed: 29224727]

Huo BX, Gao YR, and Drew PJ (2015). Quantitative separation of arterial and venous cerebral blood volume increases during voluntary locomotion. Neuroimage 105, 369–379. [PubMed: 25467301]

Huo BX, Smith JB, and Drew PJ (2014). Neurovascular coupling and decoupling in the cortex during voluntary locomotion. Journal of Neuroscience 34, 10975–10981. [PubMed: 25122897]

Huppé-Gourgues F, Karim Jegouic K, and Vaucher E (2018). Topographic organization of cholinergic innervation From the basal forebrain to the visual cortex in the rat. Frontiers of Neural Circuits 12, e00019.

Iaccarino HF, Singer AC, Martorell AJ, Rudenko A, Gao F, Gillingham TZ, Mathys H, Seo J, Kritskiy O, Abdurrob F, et al. (2016). Gamma frequency entrainment attenuates amyloid load and modifies microglia. Nature 540, 230–235. [PubMed: 27929004]

Iadecola C (2004). Neurovascular regulation in the normal brain and in Alzheimer's disease. Nature Reviews of Neuroscience 5, 347–360. [PubMed: 15100718]

Ichikawa N, Fujiwara M, Kawaguchi F, Kaga M, and Kawasak i.S. (1999). Development of optical topography system ETG-100. Dedix Report 34, 47–52.

Ilcha CP, and Golanov EV (2004). Cerebrovasodilation evoked by stimulation of subthalamic vasodilator area and hypoxia depends upon the integrity of cortical neurons in the rat. Neuroscience Letters 368, 92–95. [PubMed: 15342141]

Iliff JJ, Wang M, Liao Y, Plogg BA, Peng W, Gundersen GA, Benveniste H, Vates GE, Deane R, Goldman SA, et al. (2012). A paravascular pathway facilitates CSF flow through the brain parenchyma and the clearance of interstitial solutes, Including amyloid β. Science Translational Medicine 4, e111.

Intaglietta M (1990). Vasomotion and flowmotion: physiological mechanisms and clinical evidence. Reviews in Vascular Medicine 1, 101–112.

Kaminer J, Powers AS, Horn KG, Hu C, and Evinger C (2011). Characterizing the spontaneous blink generator: An animal model. Journal of Neuroscience 31, 11256–11267. [PubMed: 21813686]

Kay KN, Naselaris T, Prenger RJ, and Gallant JL (2008). Identifying natural images from human brain activity. Nature 452, 352–355. [PubMed: 18322462]

Keller CJ, Bickel S, Honey CJ, Groppe DM, Entz L, Craddock RC, Lado FA, Kelly C, Milham M, and Mehta AD (2013). Neurophysiological investigation of spontaneous correlated and anticorrelated fluctuations of the BOLD signal. Journal of Neuroscience 33, 6333–6342. [PubMed: 23575832]

Kim JH, Jung AH, Jeong D, Cho I, Kim K, Shin S, Kim SJ, and Lee S-H (2016a). Selectivity of neuromodulatory projections from the basal forebrain and locus ceruleus to primary sensory cortices. Journal of Neuroscience 36, 5314–5327. [PubMed: 27170128]

Kim KJ, Diaz JR, Iddings JA, and Filosa JA (2016b). Vasculo-neuronal coupling: Retrograde vascular communication to brain neurons. Journal of Neuroscience 36, 12624–12639. [PubMed: 27821575]

Kim Y, Yang GR, Pradhan K, Venkataraju KU, Bota M, Del Molino LCG, Fitzgerald G, Ram K, He M, Levine JM, et al. (2017). Brain-wide maps reveal stereotyped cell-type-based cortical architecture and subcortical sexual dimorphism. Cell 171, 456–469. [PubMed: 28985566]

Kiviniemi V, Ruohonen J, and Tervonen O (2005). Separation of physiological very low frequency fluctuation from aliasing by switched sampling interval fMRI scans. Journal of Magnetic Resonance Imaging 23, 41–46.

Kleinfeld D, Blinder P, Drew PJ, Driscoll JD, Muller A, Tsai PS, and Shih AY (2011). A guide to delineate the logic of neurovascular signaling in the brain. Frontiers in Neuroenergetics 1, 1–9.

Kleinfeld D, Mitra PP, Helmchen F, and Denk W (1998). Fluctuations and stimulus-induced changes in blood flow observed in individual capillaries in layers 2 through 4 of rat neocortex. Proceedings of the National Academy of Sciences USA 95, 15741–15746.

Knot HJ, and Nelson MT (1998). Regulation of arterial diameter and wall [Ca^{2+}] in cerebral arteries of rat by membrane potential and intravascular pressure. Journal of Physiology 508, 199–209.

Knutsen PM, Mateo C, and Kleinfeld D (2016). Precision mapping of vibrissa representation within murine primary somatosensory cortex. Philosophical Transactions of the Royal Society B 371, e20150351.

Koenigsberger M, Sauser R, Beny J-L, and Meister J-J (2006). Effects of arterial wall stress on vasomotion. Biophysical Journal 91, 1663–1674. [PubMed: 16751242]

Kopell N, and LeMasson G (1994). Rhythmogenesis, amplitude modulation, and multiplexing in a cortical architecture. Proceedings of the National Academy of Sciences USA 91, 10586–10590.

Koukouli F, Rooy M, Changeux J-P, and Maskosa U (2016). Nicotinic receptors in mouse prefrontal cortex modulate ultraslow fluctuations related to conscious processing. Proceedings of the National Academy of Sciences USA 113, 14823–14828.

Krawchuk MB, Ruff CF, Yang X, Ross SE, and Vazquez AL (2019). Optogenetic assessment of VIP, PV, SOM and NOS inhibitory neuron activity and cerebral blood flow regulation in mouse somato-sensory cortex. Journal of Cerebral Blood Flow & Metabolism, epub.

Kuramoto Y (1984). Chemical Oscillations, Waves and Turbulence (New York: Springer Verlag).

Kurnikova A, Moore JD, Liao S-M, Deschenes M, and Kleinfeld D (2017). Coordination of orofacial motor actions into exploratory behavior by rat. Current Biology 27, 1–9. [PubMed: 27916526]

Kwong KK, Belliveau KW, Chesler DA, Goldberg IE, Weisskoff RM, Poncelet BP, Kennedy DN, Hoppel BE, Cohen MS, Turner R, et al. (1992). Dynamic magnetic resonance imaging of human brain activity during sensory stimulation. Proceedings of the National Academy of Sciences USA 89, 5675–5679.

Lachaux J-P, Fonlupt P, Kahane P, Minotti L, Hoffman D, Bertrand O, and Baciu M (2007). Relationship between task-related gamma oscillations and BOLD signal: New insights from combined fMRI and intracranial EEG. Human Brian Mapping 28, 1368–1375.

Laird A, Lancaster J, and Fox P (2005). BrainMap. The social evolution of a human brain mapping database. NeuroInformatics 3, 65–77. [PubMed: 15897617]

Lear CSC, Flanagan JB Jr., and Moorrees CFA (1965). The frequency of deglutition in man. Arch Oral Biol 10, 83–99. [PubMed: 14262163]

Lee JH, Durand R, Gradinaru V, Zhang F, Goshen I, Kim DS, Fenno LE, Ramakrishnan C, and Deisseroth K (2010). Global and local fMRI signals driven by neurons defined optogenetically by type and wiring. Nature 465, 788–792. [PubMed: 20473285]

Lemon R (1984). Methods for Neuronal Recording in Conscious Animals (Chichester: John Wiley and Sons).

Leopold DA, Murayama Y, and Logothetis NK (2003). Very slow activity fluctuations in monkey visual cortex: Implications for functional brain imaging. Cerebral Cortex 13, 422–433. [PubMed: 12631571]

Li N, Daie K, Svoboda K, and Druckmann S (2016). Robust neuronal dynamics in premotor cortex during motor planning. Nature 532, 459–464. [PubMed: 27074502]

Li X, Yu B, Sun Q, Zhang Y, Ren M, Zhang X, Li A, Yuan J, Madisen L, Luo Q, et al. (2018). Generation of a whole-brain atlas for the cholinergic system and mesoscopic projectome analysis of basal forebrain cholinergic neurons. Proceedings of the National Academy of Sciences USA 115, 415–420.

Liang Z, Liu X, and Zhang N (2015). Dynamic resting state functional connectivity in awake and anesthetized rodents. NeuroImage 104, 89–99. [PubMed: 25315787]

Lieke EE, Frostig RD, Arieli A, Ts'o DY, Hildesheim R, and Grinvald A (1989). Optical imaging of cortical activity: Real-time imaging using extrinsic dye-signals and high resolution imaging based on slow intrinsic-signals. Annual Review of Physiology 51, 543–559.

Lima B, Cardoso MM, Sirotin YB, and Das A (2014). Stimulus-related neuroimaging in task-engaged subjects is best predicted by concurrent spiking. Journal of Neuroscience 34, 3878–3891. [PubMed: 24623766]

Lindauer U, Megow D, Matsuda H, and Dirnagl U (1999). Nitric oxide: a modulator, but not a mediator, of neurovascular coupling in rat somatosensory cortex. American Journal of Physiology - Heart and Circulatory Physiology 277, 799–811.

Liu X, de Zwart JA, Scholvinck ML, Chang C, Ye FQ, and Leopold DA (2018). Subcortical evidence for a contribution of arousal to fMRI studies of brain activity. Nature Communications 9, e395.

Liu X, and Duyn JH (2013). Time-varying functional network information extracted from brief instances of spontaneous brain activity. Proceedings of the National Academy of Sciences USA 110, 4392–4397.

Logothetis NK, Eschenko O, Murayama Y, Augath M, Steudel T, Evrard HC, Besserve M, and Oeltermann A (2012). Hippocampal-cortical interaction during periods of subcortical silence. Nature 491, 547–553. [PubMed: 23172213]

Logothetis NK, Pauls J, Augath M, Trinath T, and Oeltermann A (2001). Neurophysiological investigation of the basis of the fMRI signal. Nature 412, 150–157. [PubMed: 11449264]

Logothetis NK, and Wandell BA (2004). Interpreting the BOLD signal. Annual Review Physiology 66, 735–769.

Longden TA, Dabertrand F, Koide M, Gonzales AL, Tykocki NR, Brayden JE, Hill-Eubanks D, and Nelson MT (2017). Capillary K^+-sensing initiates retrograde hyperpolarization to increase local cerebral blood flow. Nature Neuroscience 20, 717–726. [PubMed: 28319610]

Lowe MJ, Mock BJ, and Sorenson JA (1998). Functional connectivity in single and multislice echoplanar imaging using resting state fluctuations. Neuroimage 7, 119–132. [PubMed: 9558644]

Lowen SB, Cash SS, Poo M, and Teich MC (1997). Quantal neurotransmitter secretion rate exhibits fractal behavior. Journal of Neuroscience 17, 5666–5677. [PubMed: 9221766]

Lu H, Golay X, Pekar JJ, and van Zij PCM (2003). Functional magnetic resonance imaging based on changes in vascular space occupancy. Magnetic Resonance in Medicine 50, 263–274. [PubMed: 12876702]

Lu H, Zou Q, Gu H, Raichle ME, Stein EA, and Yang Y (2012). Rat brains also have a default mode network. Proceedings of the National Academy of Sciences USA 109, 3979–3984.

Lv Y, Margulies DS, Craddock RC, Long X, Winter B, Gierhake D, Endres M, Kersten Villringer K, Fiebach J, and Villringer A (2012). Identifying the perfusion deficit in acute stroke with resting-state functional magnetic resonance imaging. Annals of Neurology 73, 136–139.

Ma J, Ayata C, Huang PL, Fishman MC, and Moskowitz MA (1996). Regional cerebral blood flow response to vibrissal stimulation in mice lacking type I NOS gene expression. American Journal of Physiology - Heart and Circulatory Physiology 270, 1085–1090.

Ma Y, Shaik MA, Kozberg MG, Kim SH, Portes JP, Timerman D, and Hillman EM (2016). Resting-state hemodynamics are spatiotemporally coupled to synchronized and symmetric neural activity in excitatory neurons. Proceedings of the National Academy of Sciences USA 113, 8463–8471.

Majeed W, Magnuson M, Hasenkamp W, Schwarb H, Schumacher EH, Barsalou L, and Keilholz SD (2011). Spatiotemporal dynamics of low frequency BOLD fluctuations in rats and humans. Neuroimage 54, 1140–1150. [PubMed: 20728554]

Martin RE, Goodyear BG, Gati JS, and Menon RS (2001). Cerebral cortical representation of automatic and volitional swallowing in humans. Journal of Neurophysiology 85, 938–950. [PubMed: 11160524]

Mateo C, Knutsen PM, Tsai PS, Shih AY, and Kleinfeld D (2017). Entrainment of arteriole vasomotor fluctuations by neural activity is a basis of blood oxygen level dependent “resting state” connectivity. Neuron 96, 936–948. [PubMed: 29107517]

Mathiisen TM, Lehre KP, Danbolt NC, and Ottersen OP (2010). The perivascular astroglial sheath provides a complete covering of the brain microvessels: An electron microscopic 3D reconstruction. Glia 58, 1094–1103. [PubMed: 20468051]

Mathis A, Mamidanna P, Cury KM, Abe T, Murthy VN, Mathis MW, and Bethge M (2018). DeepLabCut: Markerless pose estimation of user-defined body parts with deep learning. Nature Neuroscience 21, 1281–1289. [PubMed: 30127430]

Mayhew JEW, Askew S, Zeng Y, Porrill J, Westby GWM, Redgrave P, Rector DM, and Harper RM (1996). Cerebral vasomotion: 0.1 Hz oscillation in reflectance imaging of neural activity. Neuroimage 4, 183–193. [PubMed: 9345508]

Mishra A, Reynolds JP, Chen Y, Gourine AV, Rusakov DA, and Attwell D (2016). Astrocytes mediate neurovascular signaling to capillary pericytes but not to arterioles. Nature Neuroscience 19, 1619–1627. [PubMed: 27775719]

Mitra A, Snyder AZ, Blazey T, and Raichle ME (2015). Lag threads organize the brain’s intrinsic activity. Proceedings of the National Academy of Sciences USA 112, 2235–2244.

Mitra PP (2014). The circuit architecture of whole brains at the mesoscopic scale. Neuron 83, 1273–1283. [PubMed: 25233311]

Mitra PP, and Bokil HS (2008). Observed Brain Dynamics (New York: Oxford University Press).

Mitra PP, Ogawa S, Hu X, and Ugurbil K (1997). The nature of spatiotemporal changes in cerebral hemodynamics as manifested in functional magnetic resonance imaging. Magnetic Resonance in Medicine 37, 511–518. [PubMed: 9094072]

Mohajerani MH, Chan AW, Mohsenvand M, Ledue J, Liu R, McVea DA, Boyd JD, Wang YT, Reimers M, and Murphy TH (2013). Spontaneous cortical activity alternates between motifs defined by regional axonal projections. Nature Neuroscience 16, 1426–1435. [PubMed: 23974708]

Mohajerani MH, McVea DA, Fingas M, and Murphy TH (2010). Mirrored bilateral slow-wave cortical activity within local circuits revealed by fast bihemispheric voltage-sensitive dye imaging in anesthetized and awake mice. Journal of Neuroscience 30, 3745–3751. [PubMed: 20220008]

Moon CH, Fukuda M, and Kim SG (2013). Spatiotemporal characteristics and vascular sources of neural-specific and -nonspecific fMRI signals at submillimeter columnar resolution. Neuroimage 64, 91–103. [PubMed: 22960251]

Murphy K, Birn RM, and Bandettini PA (2013). Resting-state fMRI confounds and cleanup. Neuroimage 80, 349–359. [PubMed: 23571418]

Musall S, Kaufman MS, Juavinett AL, Gluf S, and Churchland AK (2019). Single-trial neural dynamics are dominated by richly varied movements. Nature Neuroscience 10, 1677–1686.

Nakano T, Kato M, Morito Y, Itoi S, and Kitazawa S (2013). Blink-related momentary activation of the default mode network while viewing videos. Proceedings of the National Academy of Sciences USA 110, 702–706.

Ngai AC, and Winn HR (1996). Estimation of shear and flow rates in pial arterioles during somatosensory stimulation. American Journal of Physiology - Heart and Circulatory Physiology 270, 1712–1717.

Niessing J, Ebisch B, Schmidt KE, Niessing M, Singer W, and Galuske RA (2005). Hemodynamic signals correlate tightly with synchronized gamma oscillations. Science 309, 948–951. [PubMed: 16081740]

Nir Y, Fisch L, Mukamel R, Gelbard-Sagiv H, Arieli A, Fried I, and Malach R (2007). Coupling between neuronal firing rate, gamma FLP, BOLD fMRI is related to interneuronal correlations. Current Biology 17, 1275–1285. [PubMed: 17686438]

Nir Y, Mukamel R, Dinstein I, Privman E, M. H, Fisch L, Gelbard-Sagiv H, Kipervasser S, Fani A, Neufeld MY, et al. (2008). Interhemispheric correlations of slow spontaneous neuronal fluctuations revealed in human sensory cortex. Nature Neuroscience 11, 1100–1108. [PubMed: 19160509]

Nita DA, Vanhatalo S, Lafortune F-D, Voipio J, Kaila K, and Amzica F (2004). Nonneuronal origin of CO2-related DC EEG shifts: An in vivo study in the cat. Journal of Neurophysiology 92, 1011–1022. [PubMed: 15056689]

Nizar K, Uhlirova H, Tian P, Saisan PA, Cheng Q, Reznichenko L, Weldy KL, Steed TC, B. SV, Macdonald CL, et al. (2013). In vivo stimulus-induced vasodilation occurs without IP3 receptor activation and may precede astrocytic calcium increase. Journal of Neuroscience 33, 8411–8422. [PubMed: 23658179]

Noordmans HJ, van Blooijs D, Siero JCW, Zwanenburg JJW, Klaessens JHGM, Ramsey NF, Noordmans HJ, van Blooijs D, Siero JCW, Zwanenburg JJM, et al. (2018). Detailed view on slow sinusoidal, hemodynamic oscillations on the human brain cortex by Fourier transforming oxy/deoxy hyperspectral images. Human Brain Maps 39, 3558–3573.

Obrig H, Neufang M, Wenzel R, Kohl M, Steinbrink J, Einhaupl K, and Villringer A (2000). Spontaneous low frequency oscillations of cerebral hemodynamics and metabolism in human adults. NeuroImage 12, 623–639. [PubMed: 11112395]

Ogawa S, Lee T-M, Nayak AS, and Glynn P (1990). Oxygenation-sensitive contrast in magnetic resonance image of rodent brain at high fields. Magnetic Resonance in Medicine 14, 68–78. [PubMed: 2161986]

Ogawa S, Menon RS, Tank DW, Kim SG, Merkle H, Ellermann JM, and Ugurbil K (1993). Functional brain mapping by blood oxygenation level-dependent contrast magnetic resonance imaging: A comparison of signal characteristics with a biophysical model. Biophysical Journal 64, 803–812. [PubMed: 8386018]

Ogawa S, Tank DW, Menon R, Ellermann JM, Kim S-G, Merkle H, and Ugurbil K (1992). Intrinsic signal changes accompanying sensory stimulation: Functional brain mapping with magnetic resonance imaging. Proceedings of the National Academy of Sciences USA 89, 5951–5955.

Okun M, Steinmetz N, . A., Lak A, Dervinis M, and Harris KD (2019). Distinct structure of cortical population activity on fast and infraslow timescales. Cerebral Cortex 29, 2196–2210. [PubMed: 30796825]

Osol G, and Halpern W (1988). Spontaneous vasomotion in pressurized cerebral arteries from genetically hypertensive rats. American Journal of Physiology - Heart and Circulatory Physiology 254, 28–33.

Pais-Roldan P, Biswal B, Scheffler K, and Yu X (2018). Identifying respiration-related aliasing artifacts in the rodent resting state fMRI. Frontiers in Neuroscience 12, e788.

Pan WJ, Billings JC, Grooms JK, Shakil S, and Keilholz SD (2015). Considerations for resting state functional MRI and functional connectivity studies in rodents. Frontiers in Neuroscience 5, 269.

Papoulis A (1962). The Fourier integral and its applications (New York: McGraw-Hill Book Company).

Pauling L, and Coryell CD (1936). The magnetic properties and structure of hemoglobin, oxyhemoglobin and carbonmonoxyhemoglobin. Proceedings of the National Academy of Sciences USA 22, 210–216.

Petridou N, Gaudes CC, Dryden IL, Francis ST, and Gowland PA (2013). Periods of rest in fMRI contain individual spontaneous events which are related to slowly fluctuating spontaneous activity. Human Brain Mapping 34, 1319–1329. [PubMed: 22331588]

Pinto L, Goard MJ, Estandian D, Xu M, Kwan AC, Lee SH, Harrison TC, Feng G, and Dan Y (2013). Fast modulation of visual perception by basal forebrain cholinergic neurons. Nature Neuroscience 16, 1857–1863. [PubMed: 24162654]

Pisauro MA, Dhruv NT, Carandini M, and Benucci A (2013). Fast hemodynamic responses in the visual cortex of the awake mouse. Journal of Neuroscience 33, 18343–18351. [PubMed: 24227743]

Poplawsky AJ, Fukuda M, Kang BM, Kim JH, Suh M, and Kim SG (2019). Dominance of layer-specific microvessel dilation in contrast-enhanced high-resolution fMRI: Comparison between

hemodynamic spread and vascular architecture with CLARITY. NeuroImage 197, 657–667. [PubMed: 28822749]

Power JD, Barnes KA, Snyder AZ, Schlaggar BL, and Petersen SE (2012). Spurious but systematic correlations in functional connectivity MRI networks arise from subject motion. Neuroimage 59, 2142–2154. [PubMed: 22019881]

Quigley MA, Cordes D, Turski PA, Moritz C, Haughton VM, Seth R, and Meyerand ME. (2003). Role of the corpus callosum in functional connectivity. American Journal of Neuroradiology 24, 2018–2212.

Raichle ME, MacLeod AM, Snyder AZ, Powers WJ, Gusnard DA, and Shulman GL (2001). A default mode of brain function. Proceedings of the National Academy of Sciences USA 98, 676–682.

Raj D, Paley DP, Anderson AW, Kennan RP, and Gore JC (2000). A model for susceptibility artefacts from respiration in functional echo-planar magnetic resonance imaging. Physics in Medicine and Biology 45, 3809–3820. [PubMed: 11131201]

Rasmussen R, Nicholas E, Petersen NC, Dietz AG, Xu Q, Sun Q, and Nedergaard M (2019). Cortex-wide changes in extracellular potassium ions parallel brain state transitions in awake behaving mice. Cell Repprts 28, 1182–1194.

Rayshubskiy A, Wojtasiewicz TJ, Mikell CB, Bouchard MB, Timerman D, Youngerman BE, McGovern RA, Otten ML, Canoll P, McKhann II GM, et al. (2013). Direct, intraoperative observation of~ 0.1 Hz hemodynamic oscillations in awake human cortex: Implications for fMRI. Neuroimage 87, 323–331. [PubMed: 24185013]

Reimer J, Froudarakis E, Cadwell CR, Yatsenko D, Denfield GH, and Tolias AS (2014). Pupil fluctuations track fast switching of cortical states during quiet wakefulness. Neuron 84, 355–362. [PubMed: 25374359]

Rennels ML, Gregory TF, Blaumanis OR, Fujimoto K, and Grady PA (1985). Evidence for a ‘paravascular’ fluid circulation in the mammalian central nervous system, provided by the rapid distribution of tracer protein throughout the brain from the subarachnoid space. Brain Research 326, 47–63. [PubMed: 3971148]

Revel A, Gallet C, Oréa V, Chapuis B, Barrès C, and Julien C (2012). Effect of chronic cervical ganglionectomy on the spontaneous variability of internal carotid blood flow in the conscious rat. Experimental Psychology 97, 564–571.

Rosenegger DG, Tran CH, Wamsteeker Cusulin JI, and Gordon GR (2015). Tonic local brain blood flow control by astrocytes independent of phasic neurovascular coupling. Journal of Neuroscience 35, 13463–13474. [PubMed: 26424891]

Sakaguchi H, Shinomoto S, and Kuramoto Y (1988). Mutual entrainment in oscillator lattices with nonvariational type interaction. Progress of Theoretical Physics 79, 1069–1079.

Salkoff D,B, Zagha E, McCarthy E, and McCormick DA (2019). Movement and performance explain widespread cortical activity in a visual detection task. Cerebral Cortex, epub.

Saper CB (1984). Organization of cerebral cortical afferent systems in the rat. II. Magnocellular basal nucleus. Journal of Comparative Neurology 222, 313–342.

Sato A, Sato Y, and Uchida S (2001). Regulation of regional cerebral blood flow by cholinergic fiber originating in the basal forebrain. International Journal of Developmental Neuroscience 19, 327–337. [PubMed: 11337202]

Schölvinck ML, Maier A, Ye FQ, Duyn JH, and Leopold DA (2010). Neural basis of global resting-state fMRI activity. Proceedings of the National Academy of Sciences USA 107, 10238–10243.

Schölvinck ML, Saleem AB, Benucci A, Harris KD, and Carandini M (2015). Cortical state determines global variability and correlations in visual cortex. Journal of Neuroscience 35, 170–178. [PubMed: 25568112]

Schulz K, Sydekum E, Krueppel R, Engelbrecht CJ, Schlegel F, Schröter A, Rudin M, and Helmchen F. (2012). Simultaneous BOLD fMRI and fiber-optic calcium recording in rat neocortex. Nature Methods 9, 597–602. [PubMed: 22561989]

Schwalm M, Schmid F, Wachsmuth L, Backhaus H, Kronfeld A, Jury FA, Prouvot PH, Fois C, Albers F, van Alst Tv et al. (2017). Cortex-wide BOLD fMRI activity reflects locally-recorded slow oscillation-associated calcium waves. eLife 6, e27602. [PubMed: 28914607]

Segal SS, and Duling BR (1989). Conduction of vasomotor responses in arterioles: A role for cell-to-cell coupling? American Journal of Physiology - Heart and Circulatory Physiology 256, 838–845.

Semba K, Reiner PB, McGeer EG, and Fibiger HC (1988). Non-cholinergic basal forebrain neurons project to the contralateral basal forebrain in the rat. Neuroscience Letters 84, 23–28. [PubMed: 2831483]

Şencan I, Esipova T, Kılıç K, Li B, Desjardins M, Yaseen MA, Wang H, Porter JE, Kura S, Fu B, et al. (2020). Optical measurement of microvascular oxygenation and blood flow responses in awake mouse cortex during functional activation. Journal of Cerebral Blood Flow & Metabolism, OnlineFirst.

Shmuel A, Augath M, Oeltermann A, and Logothetis NK (2006). Negative functional MRI response correlates with decreases in neuronal activity in monkey visual area V1. Nature Neuroscience 9, 569–577. [PubMed: 16547508]

Shmuel A, and Leopold DA (2008). Neuronal correlates of spontaneous fluctuations in fMRI signals in monkey visual cortex: Implications for functional connectivity at rest. Human Brain Mapping 29, 751–761. [PubMed: 18465799]

Shmueli K, van Gelderen P, de Zwart JA, Horovitz SG, Fukunaga M, Jansma JM, and Duyn JH (2007). Low-frequency fluctuations in the cardiac rate as a source of variance in the resting-state fMRI BOLD signal. Neuroimage 38, 306–320. [PubMed: 17869543]

Shulman RG, Hyder F, and Rothman DL (2002). Biophysical basis of brain activity: Implications for neuroimaging. Quarterly Reviews of Biophysics 35, 287–325. [PubMed: 12599751]

Siegel JS, Power JD, Dubis JW, C NA, Church JA, Schlaggar BL, and Petersen SE(2014). Statistical improvements in functional magnetic resonance imaging analyses produced by censoring high-motion data points. Human Brain Mapping 35, 1981–1996. [PubMed: 23861343]

Sirotin YB, Hillman EM, Bordier C, and Das A (2009). Spatiotemporal precision and hemodynamic mechanism of optical point spreads in alert primates. Proceedings of the National Academy of Sciences USA 106, 18390–18395.

Smith SM, Fox PT, Miller KL, Glahn DC, Fox PM, Mackay CE, Filippini N, Watkins KE, Toro R, Laird AR, et al. (2009). Correspondence of the brain's functional architecture during activation and rest. Proceedings of the National Academy of Sciences USA 106, 13040–13045.

Sofroniew NJ, Flickinger D, King J, and Svoboda K (2016). A large field of view two-photon mesoscope with subcellular resolution for in vivo imaging. eLife 5, e14472. [PubMed: 27300105]

Sohal VS, Zhang F, Yizhar O, and Deisseroth K (2009). Parvalbumin neurons and gamma rhythms enhance cortical circuit performance. Nature 459, 698–702. [PubMed: 19396159]

Sompolinsky H, Golomb D, and Kleinfeld D (1991). Cooperative dynamics in visual processing. Physical Review A 43, 6990–7011.

Sorensen SC, and Severinghaus JW (1970). Effect of cerebral acidosis on the CSF-blood potential difference. American Journal of Physiology 219, 68–71.

Sporns O, Tononi G, and Kotter R (2005). The human connectome: A structural description of the human brain. Public Library of Science Computational Biology 1, e42. [PubMed: 16201007]

Stafford JM, Jarrett BR, Miranda-Dominguez O, Mills BD, Cain N, Mihalas S, Lahvis GP, Lattal KM, Mitchell SH, David SV, et al. (2014). Large-scale topology and the default mode network in the mouse connectome. Proceedings of the National Academy of Sciences USA 111, 18745–18750.

Steinmetz NA, Buetfering C, Lecoq J, Lee CR, Peters AJ, Jacobs EAK, Coen P, Ollerenshaw DR, Valley MT, de Vries SEJ, et al. (2017). Cortical activity in multiple GCaMP6-expressing transgenic mouse lines. eNeuro 4, e0207.

Stephan SE, Harrison LM, Penny WD, and Friston KJ (2004). Biophysical models of fMRI responses. Current Opinion in Neurobiology 14, 629–635. [PubMed: 15464897]

Stergiopulos N, Porret C-A, De Brouwer S, and Meister J-J (1998). Arterial vasomotion: Effect of flow and evidence of nonlinear dynamics. American Journal of Physiology - Heart and Circulatory Physiology 274, 1858–1864.

Steriade M, Contreras D, Dossi RC, and Nunez A (1993). The slow (<1 Hz) oscillation in reticular thalamic and thalamocortical neurons: Scenario of sleep rhythm generation in interacting thalamic and neocortical networks. Journal of Neuroscience 13, 3284–3299. [PubMed: 8340808]

Stringer C, Pachitariu M, Steinmetz N, Reddy CB, Carandini4 M, and Harris KD. (2019). Spontaneous behaviors drive multidimensional, brainwide activity. Science 364, 1–11.

Strogatz SH, and Mirolla RE (1988). Phase-locking and critical phenomena in lattices of coupled nonlinear oscillators with random intrinsic frequencies. Physica D 31, 143–168.

Tagliazucchi E, and Laufs H (2014). Decoding wakefulness levels from typical fMRI resting-state data reveals reliable drifts between wakefulness and sleep. Neuron 82, 695–708. [PubMed: 24811386]

Thompson GJ, Merritt MD, Pan W-J, Magnuson ME, Grooms JK, Jaeger D, and Keilhoiz SD (2013). Neural correlates of time-varying functional connectivity in the rat. Neuroimage 83, 826–836. [PubMed: 23876248]

Thompson GJ, Pan WJ, Magnuson ME, Jaeger D, and Keilholz SD (2014). Quasi-periodic patterns (QPP): large-scale dynamics in resting state fMRI that correlate with local infraslow electrical activity. Neuroimage 84, 1018–1031. [PubMed: 24071524]

Tian P, Teng I, May LD, Kurz R, Lu K, Scadeng M, Hillman EM, De Crespigny AJ, D'Arceuil HE, Mandeville JB, et al. (2010). Cortical depth-specific microvascular dilation underlies laminar differences in blood oxygenation level-dependendent functional MRI signal. Proceedings of the National Academy of Sciences USA 107, 15246–15251.

Toib A, Lyakhov V, and Marom S (1998). Interaction between duration of activity and time course of recovery from slow inactivation in mammalian brain Na channels. Journal of Neuroscience 18, 1893–1903. [PubMed: 9465014]

Tong Y, Hocke LM, Fan X, Janes AC, and de Frederick B (2015). Can apparent resting state connectivity arise from systemic fluctuations? Frontiers in Human Neuroscience 9, e285.

Tong Y, Yao JF, Chen JJ, and Frederick BD (2019). The resting-state fMRI arterial signal predicts differential blood transit time through the brain. Journal of Cerebral Blood Flow and Metabolism 39, 1148–1160. [PubMed: 29333912]

Tsai PS, Mateo C, Field JJ, Schaffer CB, Anderson ME, and Kleinfeld D (2015). Ultra-large field-of-view two-photon laser scanning microscopy. Optics Express 23, 13833–13847. [PubMed: 26072755]

Tsitoura C, Malinowski S, Mohrhardt J, Degen R, DiBenedictis BT, Gao Y, Watznauer K, Gerhold K, Nagel M, Weber M, et al. (2020). Synchronous infra-slow oscillations organize ensembles of accessory olfactory bulb projection neurons into distinct microcircuits. Journal of Neuroscience 40, 4203–4218. [PubMed: 32312886]

Turch J, Chang C, Ye FQ, Russ BE, Yu DK, Cortes CR, Monosov IE, Duyn JH, and Leopold DA (2018). The basal forebrain regulates global resting-state fMRI fluctuations. Neuron 97, 940–952. [PubMed: 29398365]

Tyszka JM, Kennedy DP, Adolphs R, and K. PL. (2011). Intact bilateral resting-state networks in the absence of the corpus callosum. Journal of Neuroscience 31, 15154–15162. [PubMed: 22016549]

Uhlirova H, Kılıç K, Tian P, Thunemann M, Desjardins M, Saisan PA, Sakadžić S, Ness TV, Mateo C, Cheng Q, et al. (2016). Cell type specificity of neurovascular coupling in cerebral cortex. eLife 5, e14315. [PubMed: 27244241]

Uludağ K, Müller-Bierl B, and Uğurbil K (2009). An integrative model for neuronal activity-induced signal changes for gradient and spin echo functional imaging. Neuroimage 48, 150–165. [PubMed: 19481163]

Van de Moortele PF, Pfeuffer J, Glover GH, and Ugurbil K (2002). Respiration-induced B0 fluctuations and their spatial distribution in the human brain at 7 Tesla. Magnetic Resonance in Medicine 47, 888–895. [PubMed: 11979567]

van Gelderen P, de Zwart JA, Starewicz P, Hinks RS, and Duyn JH (2007). Real-time shimming to compensate for respiration-induced B0 fluctuations. Magnetic Resonance in Medicine 57, 362–368. [PubMed: 17260378]

van Veluw SJ, Hou SS, Calvo-Rodriguez M, Arbel-Ornath M, Snyder AC, Frosch MP, Greenberg SM, and Bacskai BJ (2020). Vasomotion as a driving force for paravascular clearance in the awake mouse brain. Neuron, epub.

van Vreeswijk C, Abbott LF, and Ermentrout GB (1994). When inhibition not excitation synchronizes neural firing. Journal of Computational Neuroscience 4, 313–321.

Vanhataloa S, Tallgrena P, Beckerc C, Holmesc MD, Millerc JW, Kailaa K, and Voipio J (2003). Scalp-recorded slow EEG responses generated in response to hemodynamic changes in the human brain. Clinical Neurophysiology 114, 1744–1754. [PubMed: 12948805]

Vanni MP, Chan AC, Balbi M, Silasi G, and Murphy TH (2017). Mesoscale mapping of mouse cortex reveals frequency-dependent cycling between distinct macroscale functional modules. Journal of Neuroscience 37, 7513–7533. [PubMed: 28674167]

Vaucher E, and Hamel E (1995). Cholinergic basal forebrain neurons project to cortical microvessels in the rat: Electron microscopic study with anterogradely transported phaseolus vu/gis leucoagglutinin and choline acetyltransferase immunocytochemistry. Journal of Neuroscience 15, 7427–7441. [PubMed: 7472495]

Villringer A, and Dirnagl U (1995). Coupling of brain activity and cerebral flood flow: Basis of functional neuroimaging. Cerebrovascular and Brain Metabolism Reviews 7, 240–276. [PubMed: 8519605]

Villringer A, Kempf F, Haux D, Boden S, and Obriga H (2006). Illuminating the BOLD signal: Combined fMRI-fNIRS studies. Journal of Magnetic Resonance Imaging 24, 495–505.

Vincent JL, Patel GH, Fox MD, Snyder AZ, Baker JT, Van Essen DC, Zempel JM, Snyder LH, Corbetta M, and Raichle ME (2007). Intrinsic functional architecture in the anaesthetized monkey brain. Nature 447, 83–86. [PubMed: 17476267]

Voipio J, Tallgren P, Heinonen E, Vanhatalo S, and Kaila K (2003). Millivolt-scale DC shifts in the human scalp EEG: Evidence for a nonneuronal generator. Journal of Neurophysiology 89, 2208–2214. [PubMed: 12612037]

Wang M, He Y, Sejnowski TJ, and Yu X (2018). Brain-state dependent astrocytic Ca(2+) signals are coupled to both positive and negative BOLD-fMRI signals. Proceedings of the National Academy of Sciences USA 115, 1647–1656.

Welsh DG, Tran CHT, Hald BO, and M. S (2018). The conducted vasomotor response: function, biophysical basis, and pharmacological control. Annual Reviews of Pharmacology and Toxacology 58, 391–410.

Whishaw BK, and IQ Whishaw IQ (2014). An introduction to brain and behavior (Worth Publishers).

White JA, Banks MI, Pearce RA, and Kopell NJ (2000). Networks of interneurons with fast and slow gamma-aminobutyric acid A (GABA-a) kinetics provide substrate for mixed gamma-theta rhythm. Proceedings of the National Academy of Sciences USA 97.

Whittington MA, Traub RD, and Jeffreys JG (1995). Synchronized oscillations in interneuron networks driven by metabotrophic glutamate receptor activation. Nature 373, 612–615. [PubMed: 7854418]

Williams KA, Magnuson M, Majeed W, LaConte SM, Peltier SJ, Hu X, and Keilholz SD (2010). Comparison of alpha-chloralose, medetomidine and isoflurane anesthesia for functional connectivity mapping in the rat. Journal of Magnetic Resonance Imaging 28, 995–1003.

Winder AT, Echagarruga C, Zhang Q, and Drew PJ (2017). Spontaneous hemodynamic signals report a mixture of behavior, local neural activity, and putatively non-neural processes. Nature Neuroscience 20, 1761–1769. [PubMed: 29184204]

Wise RG, Ide K, Poulin MJ, and Tracey I (2004). Resting fluctuations in arterial carbon dioxide induce significant low frequency variations in BOLD signal. Neuroimage 21, 1652–1664. [PubMed: 15050588]

Wu H, Williams J, and Nathans J (2014). Complete morphologies of basal forebrain cholinergic neurons in the mouse. eLife 3, e02444. [PubMed: 24894464]

Yamada M, Lamping KG, Duttaroy A, Zhang W, Cui Y, Bymaster FP, McKinzie DL, Felder CC, Deng C-X, Faraci FM, et al. (2001). Cholinergic dilation of cerebral blood vessels is abolished in M5 muscarinic acetylcholine receptor knockout mice. Proceedings of the National Academy of Sciences USA 98, 14096–14101.

Yan CG, Cheung B, Kelly C, Colcombe S, Craddock RC, Di Martino A, Li Q, Zuo XN, Castellanos FX, and Milham MP (2013). A comprehensive assessment of regional variation in the impact of

head micromovements on functional connectomics. Neuroimage 76, 183–201. [PubMed: 23499792]

Yeung MKS, and Strogatz SH (1999). Time delay in the Kuramoto model of coupled oscillators. Physical Review Letters 82, 648–651.

Yu J, Gutnisky DA, Hires SA, and Svoboda K (2016). Layer 4 fast-spiking interneurons filter thalamocortical signals during active somatosensation. Nature Neuroscience, 1647–1657. [PubMed: 27749825]

Yu X, Glen D, Wang S, Dodd S, Hirano Y, Saad Z, Reynolds R, Silva AC, and Koretsky AP (2012). Direct imaging of macrovascular and microvascular contributions to BOLD fMRI in layers IV-V of the rat whisker-barrel cortex. Neuroimage 59, 1451–1460. [PubMed: 21851857]

Yu X, Qian C, Chen DY, Dodd SJ, and Koretsky AP (2014). Deciphering laminar-specific neural inputs with line-scanning fMRI. Nature Methods 11, 55–58. [PubMed: 24240320]

Yüzgeç Ö, Prsa M, Zimmermann R, and Huber D (2018). Pupil size coupling to cortical states protects the stability of deep sleep via parasympathetic modulation. Current Biology 28, 392–400. [PubMed: 29358069]

Zaborszky L, Csordas A, Mosca K, Kim J, Gielow MR, Vadasz C, and Nadasdy Z (2015). Neurons in the basal forebrain project to the cortex in a complex topographic organization that reflects corticocortical connectivity patterns: an experimental study based on retrograde tracing and 3D reconstruction. Cerebral Cortex 25, 118–137. [PubMed: 23964066]

Zeng H (2018). Mesoscale connectomics. Current Opinion in Neurobiology 50, 154–162. [PubMed: 29579713]

Zerbi V, Floriou-Servou A, Markicevic M, Vermeiren Y, Sturman O, Privitera M, von Ziegler L, David Ferrari KD, Weber B, De Deyn PP, et al. (2019). Rapid reconfiguration of the functional connectome after chemogenetic locus coeruleus activation. Neuron 103, 702–718. [PubMed: 31227310]

Zhang Q, Roche M, Gheres KW, Chaigneau E, Kedarasetti RT, Haselden WD, Charpak S, and Drew PJ (2019). Cerebral oxygenation during locomotion is modulated by respiration. Nature Communications 10, e5515.

Zhao F, Zhao T, Zhou L, Wu Q, and Hu X (2008). BOLD study of stimulation-induced neural activity and resting-state connectivity in medetomidine-sedated rat. NeuroImage 39, 248–260. [PubMed: 17904868]

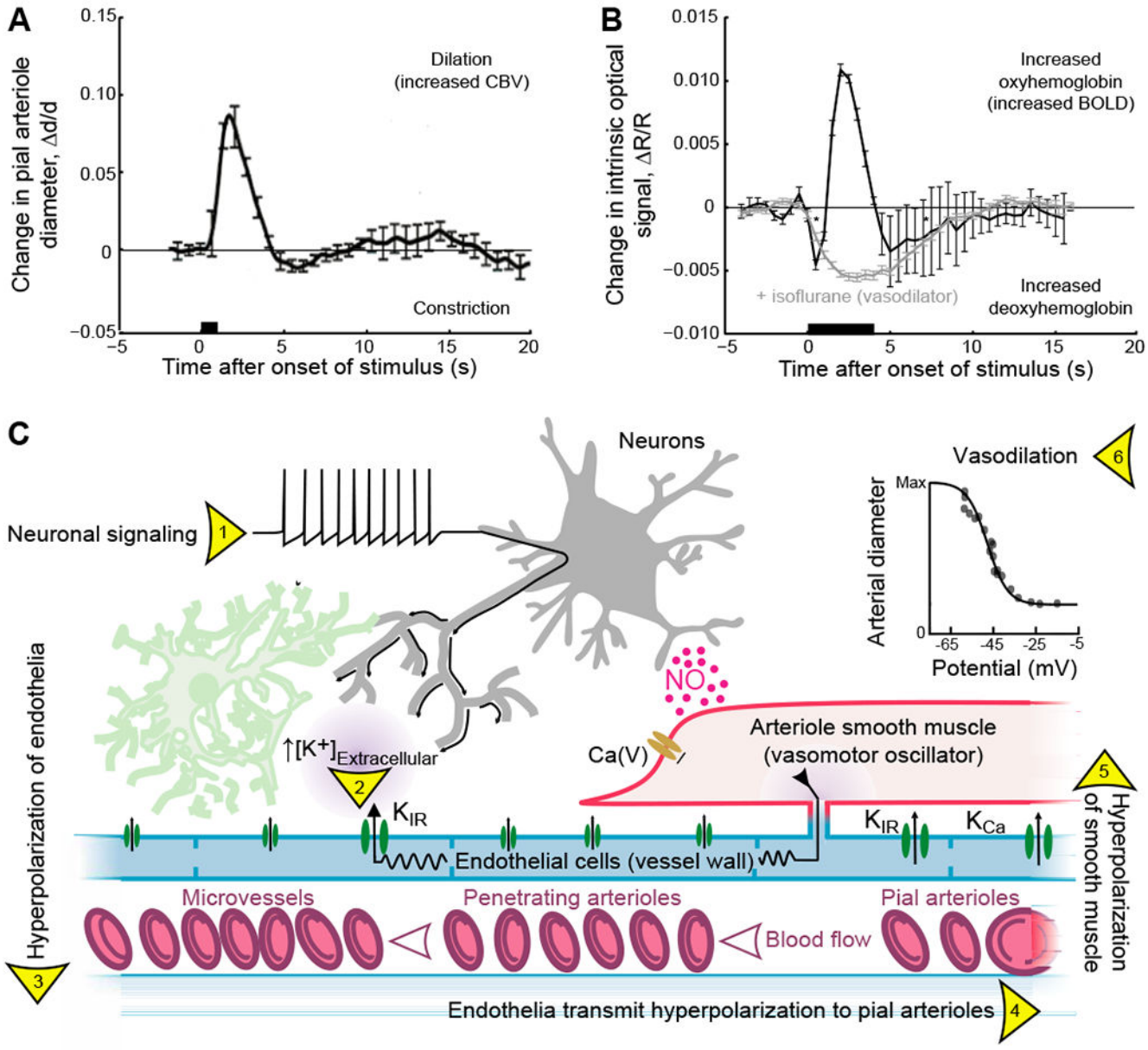

Figure 1. The neocortical vascular response to phasic sensory stimulation and the mechanism for fast neurovascular coupling

(A) The canonical effect of neuronal activity on the diameter of pial vessels as measured with two-photon laser scanning microscopy (Kleinfeld et al., 1998) using a head-fixed rat. The stimulus is a 500 ms puff to the vibrissae. Adapted rom (Uhlirova et al., 2016)

(B) The canonical effect of neuronal activity on hemodynamics as measured with intrinsic optical imaging using 630 nm light (Grinvald et al., 1988) using a head-fixed mouse. The stimulus is a 4 s puff to the vibrissae. The isoflurane data refers to a breathing mixture of 1.8 % (v/v) isoflurane in oxygen. Adapted from (Knutsen et al., 2016).

(C) Rapid mechanisms for communication of neuronal activity to drive smooth muscle hyperpolarization and arteriole dilation. Neural activity (1) leads to an increase in K^+ in the perivascular space surrounding microvessels that activates the potassium inward rectifier (2),

K_{IR}, to generate a local hyperpolarization of the endothelial membrane (3). The hyperpolarization spreads to adjacent endothelial cells through gap junctions to activate K_{IR} currents in adjacent cells (4). This results in a propagating signal from microvessels to penetration arterioles and finally surface or pial vessels. The hyperpolarization spreads to adjacent smooth muscle cells (5) and deactivates voltage-dependent Ca^{2+} currents, Ca(V), to induce smooth muscle relaxation and arteriolar dilation (6). Rapid arteriole dilation is also induced by binding of nitric oxide (NO) that is released from some inhibitory neurons, as well as other brain cells, i.e., endothelial cells, astrocytes, and microglia. The increase in arteriole diameter (panel A) can lead to an increase in blood flow. Adapted from (Longden et al., 2017) and (Knot and Nelson, 1998).

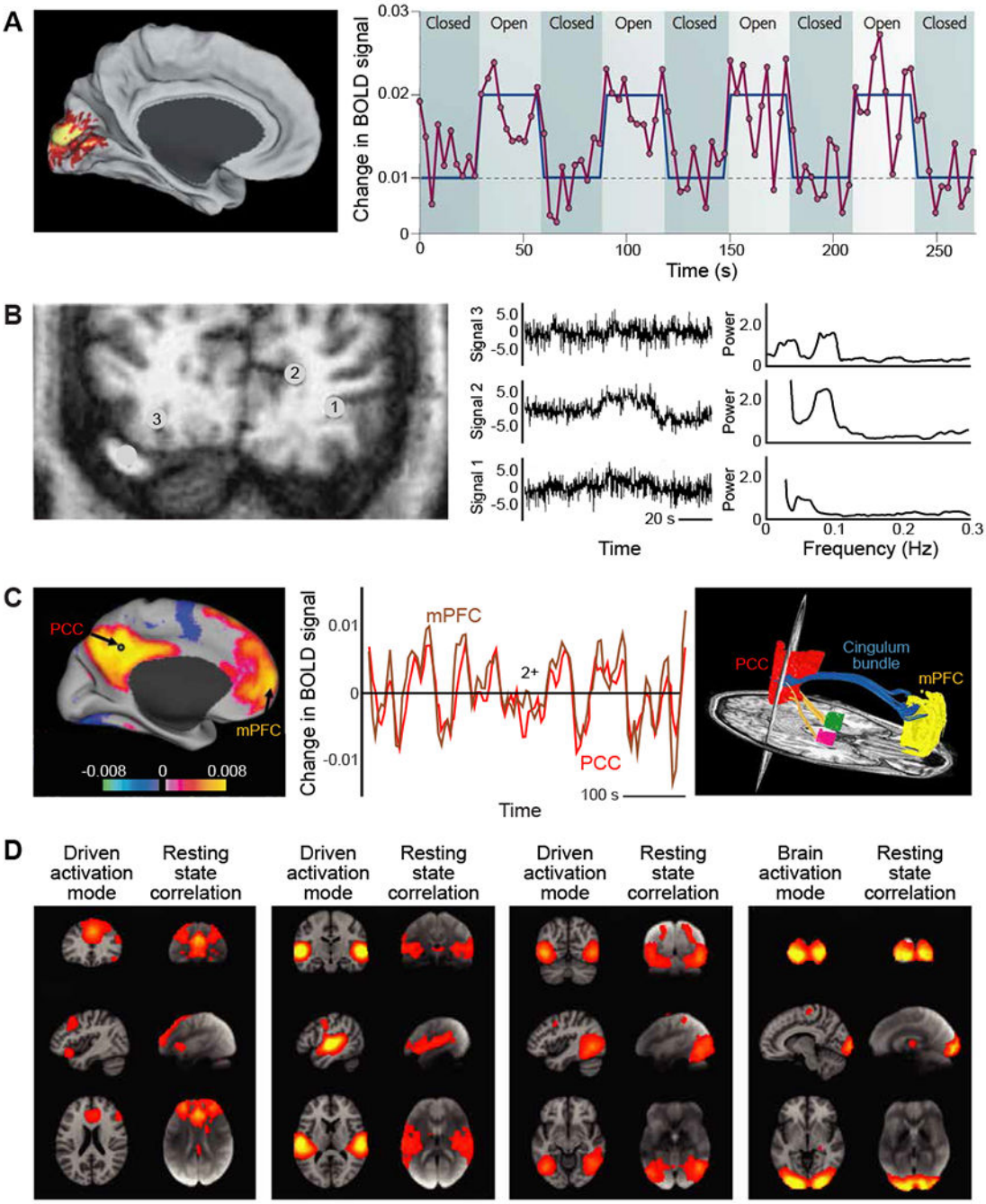

Figure 2. Functional MRI (fMRI) uses correlation in the fluctuations of signal strength to infer brain regions that are directly connected.

(A) Changes in the basic blood oxygenation level dependent (BOLD) fMRI signals generated in human visual cortex in response to changes in luminance in a full field visual input. Unaveraged BOLD signal (magenta) was obtained from a region in the primary visual cortex during a task that required subjects to open and close their eyes. The task is shown in blue, and the times are delayed to account for the hemodynamic response. The subtraction of the eyes-closed condition from the eyes-open condition identifies a BOLD signal intensity

difference in the primary visual cortex (shown on the right). Note the variability as well as the average increase in signal amplitude upon stimulation. From (Fox and Raichle, 2007).
(B) Blood oxygenation level dependent fMRI signals were obtained from a coronal slice, 2.8 cm from the occipital pole (left). Three unprocessed time courses of the BOLD fMRI signal of representative voxels, numbers 1-3 and located outside of visual cortex, and their corresponding frequency spectra (right). A binocular visual stimulus, provided by a pair of flickering red LED patterns, was on during the 40 - 70 s time interval of the 110 s period and drives voxel 4; data not reproduced here. From (Mitra et al., 1997).
(C) The BOLD fMRI signals recorded from two distant regions in human cortex, the posterior cingulate / precuneus cortex (PCC) and the medial prefrontal cortex (mPFC), are highly correlated on the time scale of tens to hundreds of seconds. Correlations are calculated between a seed voxel in the PCC and all other voxels in the brain for a single subject during rest. The spatial distribution of correlation coefficients shows both positive and negative values and was thresholded at $R^2 = 0.1$ (left image). The time course for a single run is shown for the seed region (PCC) and a region (mPFC) positively correlated with this seed region. The functional connection between the PCC and the mPFC is consistent with a fiber track revealed by diffusion tensor imaging (blue trace in right image). Left and center panels from (Fox et al., 2005), right panel from (Greicius et al., 2009).
(D) Four well-matched pairs of resting-state subnetworks that show a close correspondence between the independent analyses of activated (left column) and resting-state (right columns) brain dynamics. Activation data is from the 20-component analysis of the 29,671-subject BrainMap activation database (Fox and Lancaster, 2002; Laird et al., 2005) and resting-state data is from a separate analysis of a 36-subject resting-state fMRI dataset (Smith et al., 2009). Shown are the three most informative orthogonal slices for each pair. Left columns: network from BrainMap, shown superimposed on the MNI152 standard space template image. Right columns: resting-state fMRI data, shown superimposed on the mean fMRI image from all subjects. From (Smith et al., 2009).

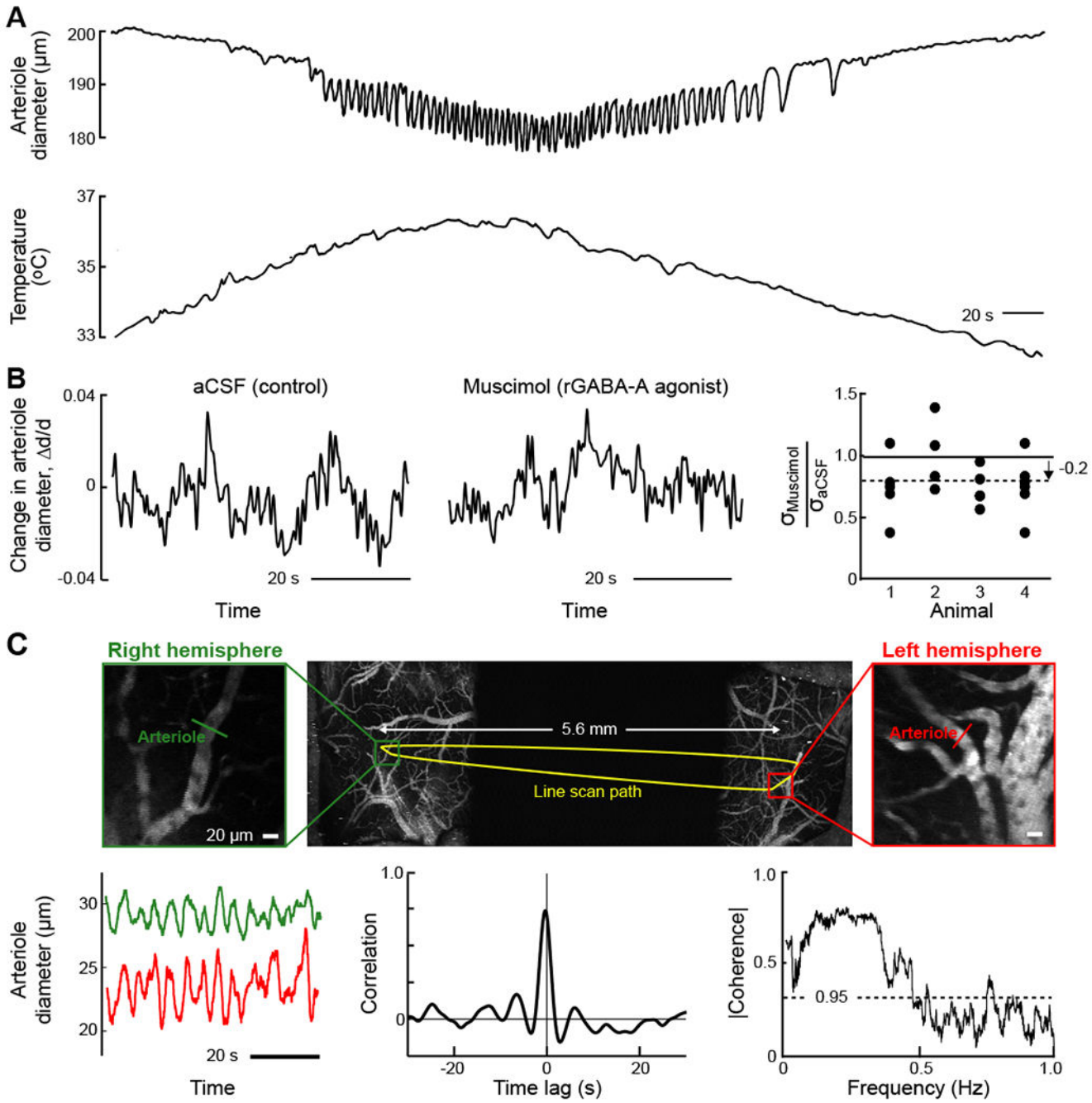

Figure 3. In vitro and in vivo measurements of vasomotion, a rhythmic change in arteriole diameter with a broad band intrinsic frequency centered near 0.1 Hz

(A) Simultaneous recording of lumen diameter (top) and temperature (bottom) in a cerebral artery that was isolated from a spontaneously hypertensive, stroke-prone rat and pressurized to 80 mmHg. Diameter oscillations appear when the artery is warmed above 35°C. From (Osol and Halpern, 1988).

(B) Example of normalized diameter measurements from a single pial arteriole with two-photon laser scanning microscopy following local artificial cerebral spinal fluid (aCSF)

infusion (left) and muscimol infusion (center) infusions in a single animal. The population summary of the root-mean-square deviation in pial arteriole diameter after muscimol infusion (19 vessels from 4 animals); oscillation amplitudes were reduced following infusion of muscimol compared to aCSF. From (Winder et al., 2017).

(C) Two-photon imaging of vasomotion in cortical arterioles across both hemispheres of an awake, head-fixed mouse. A maximally projected image stack across 500 μm of the preparation was obtained with ultra-large field-of-view two-photon microscopy (Tsai et al., 2015) (top row); the dark region in the middle corresponds to a physical mask. The arbitrary-line-scan path of the beam (yellow) spans both hemispheres. The expanded images (middle row) are single planes in each hemisphere and serve to highlight the path of the line-scan through individual vessels whose diameters were concurrently monitored. Vasomotor oscillations measured simultaneously from pial arteries in the right (green) and left (red) hemispheres appear synchronous (middle panel in middle layer). The full data set of 600 s is seen to be correlated with a lag time at the peak of 0.0 ± 0.1 s (lower row left panel). The spectral coherence in the diameter from pairs of arterioles (24 traces of 540 s traces), calculated with a bandwidth of 0.04 Hz as an average over 24 measurements. From (Tsai et al., 2015).

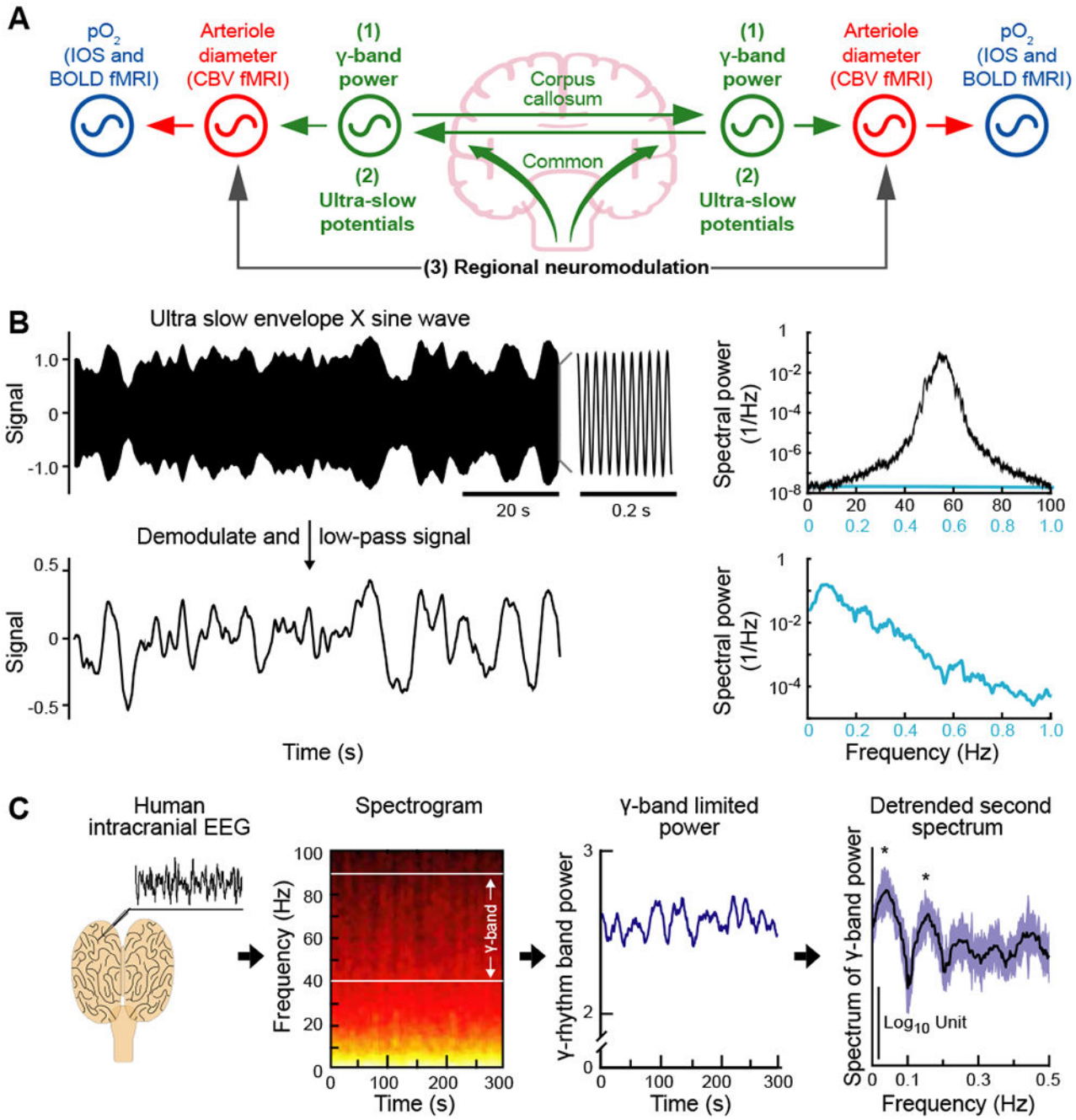

Figure 4. Ultra-slowly varying neuronal signals have multiple potential origins but are predominantly encoded by the ultra-slow modulation of the fast, γ-band oscillations.

(A) Coupled oscillator model for resting-state neurovascular coupling. The three potential coupling mechanisms for entrainment of vasomotor oscillations across separate regions of the brain: (1) the ultra-slow envelope of the γ-band oscillations shared across separate regions, as illustrated in panel B; (2) ultra-slow electrical potentials per se that are shared across separate regions; and (3) regional-specific neuromodulation of brain activity. Adapted from (Mateo et al., 2017).

(B) A model to illustrate amplitude modulation using an ultra-slow signal to modulate a fast underlying oscillatory signal. The top trace is the product of a carrier centered at $f\gamma$ = 55 Hz and a 0.1 - 0.2 Hz band-limited noise source for the ultra-slow modulate. The associated spectrum was computed with a bandwidth of 0.5 Hz (black trace) or 0.05 Hz (blue trace). The bottom trace shows the frequency components of the ultra-slow envelope after demodulation and low-pass filtering to remove signals near $2f_g$. The associated spectrum was computed with a bandwidth of 0.05 Hz. From (Mateo et al., 2017).
(C) Measurements and analysis of ultra-slow variations in the power of the surface ECoG during stage 2 sleep in a human subject (left panel); from (Nir et al., 2008). The spectrogram of the ECoG shows the slow variation in power in the 40 to 90 Hz γ-band (left-of-center panel); window of 10 s, bandwidth of 1.5 Hz, and color scales the logarithm of power from black/red (low) to white/yellow (high). The time-series of the variation of integrated power in the γ-band of the ECoG shows oscillations on the 10-s time scale. The spectrum of the derivative of this time-series, a procedure that remove a power $\propto 1/f^2$ trend from the spectrum, has statistically significant peaks at frequencies near ~ 0.1 Hz. Reanalysis from (Drew et al., 2008).

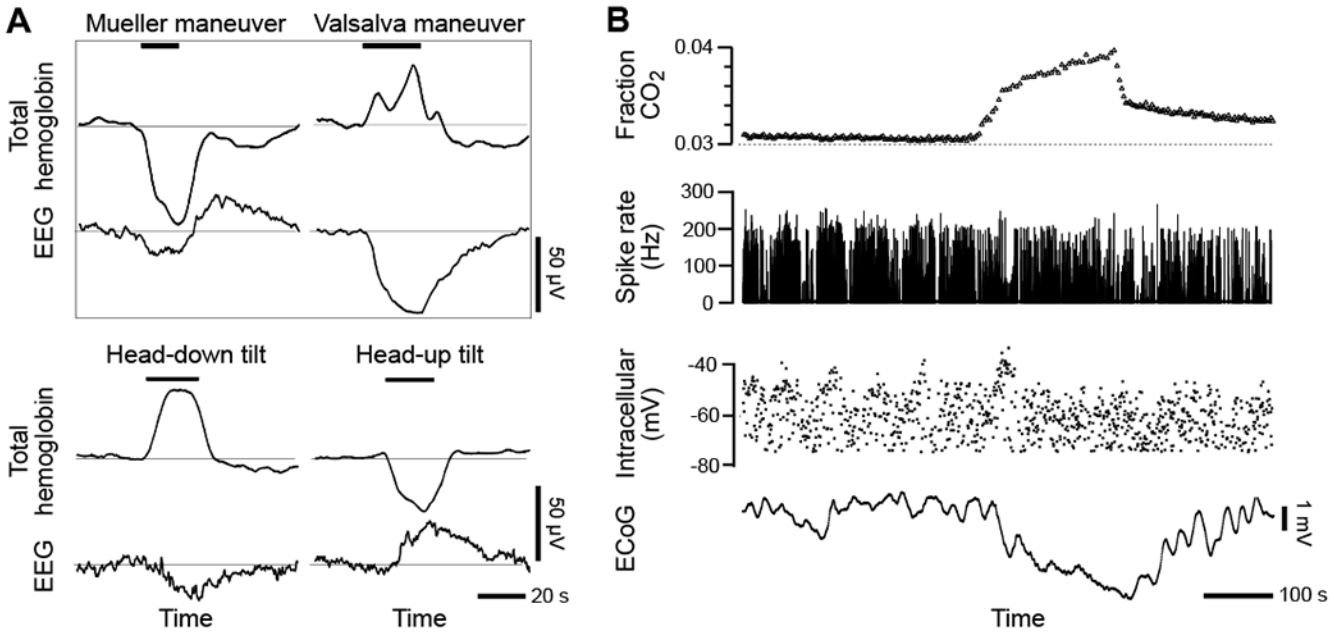

Figure 5. Ultra-slowly varying extracellular potentials, i.e., "DC potentials", can have a non-neuronal origin.

(A) Four changes in human body position that alter cerebral blood volume, i.e., Mueller and Vasalva maneuvers and head tilt maneuvers, drive changes in EEG potential as measured with scalp electrodes. The change in total blood volume was found from near infrared absorption of brain blood perfusion using scalp emitters and detectors (Ichikawa et al., 1999). The EEG scalp electrodes were at the 10-20 international coordinates Cz - (T3 + T4) for Mueller and Vasalva, Fz - (right mastoid) for head up and Cz - (right mastoid) for head down. From (Vanhataloa et al., 2003).

(B) Inhalation of CO_2, a vasodilator, drives a large shift in ECoG potentials with no effect on the transmembrane potential or spike rate of a simultaneously recorded neuron. Intracellular and DC ECoG recording during recurrent spike-wave seizures and hypoventilation in a cat under ketamine–xylazine anesthesia. From (Nita et al., 2004).

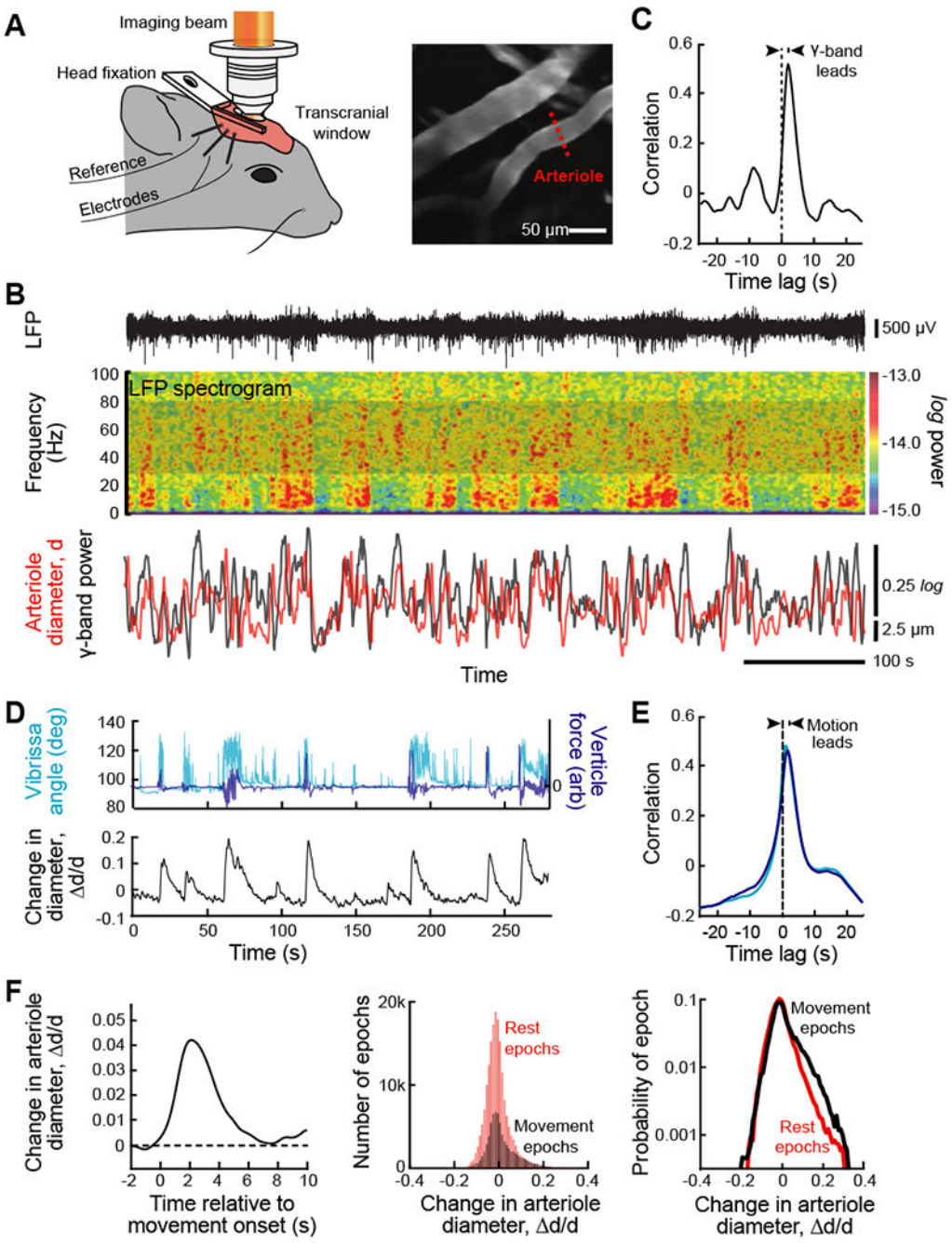

Figure 6. The envelope of neuronal γ-band oscillations locks to and leads vasomotor oscillations in arteriole diameter.

(A) Set-up with a head-fixed awake but resting mouse for two-photon imaging of arteriole diameter along with measurement of the LFP (left panel). A thinned skull window was used to preserve vasomotion (Drew et al., 2010). Two-photon images of surface vessels and scan path to define lumen diameter (center panel). From (Mateo et al., 2017).

(B) Example data showing the LFP (top trace), the spectrogram of the LFP with a window of 2.0 s and a bandwidth of 2.5 Hz, and the time series of the integrated γ-band power and diameter for one arteriole in the field (bottom traces). From (Mateo et al., 2017).
(C) The cross correlation of the two time series used for the example of panel B, 600 s total time, show that the LFP leads the diameter change. As an average across animals, movement proceeds the vasodilation by 1.9 ± 0.2 s (82 vessels from 27 mice with 600 s of data per vessel). From (Mateo et al., 2017).
(D) New data on the recording of self-generated, i.e., spontaneous movement in a head-fixed awake but resting mouse, obtained concurrent with two-photon imaging of arteriole diameter (Winder et al., 2017) similar to that in panel A, to determine the possible contribution of such movement to the entrainment of vasomotion. Bouts of whisking were determined with videography and whole-body vertical acceleration determined with a force sensor attached to the tube supporting the mouse's body.
(E) Correlation analysis of new data (27 vessels from 9 mice with 1700 to 12000 s of data per vessel). The time-lag of the correlation shows that movement leads the change in diameter (bottom panel) with lag times similar to that for movement proceeds the vasodilation by 1.8 ± 0.3 s for whisking and 1.5 ± 0.3 s for whole body motion.
(F) A re-analysis of the data of Mateo et al. (2017), similar to that for the new data of panels E and F, using previously unpublished simultaneous measurements of the whole body horizontal acceleration acquired during imaging (82 vessels from 27 mice). Accelerations lead to a change in arteriole diameters (left panel); the threshold detectability was ~ 0.01 g. Theses movement related changes in diameter are compared to rest events (middle panel) and dominate the largest changes in diameter (right panel).

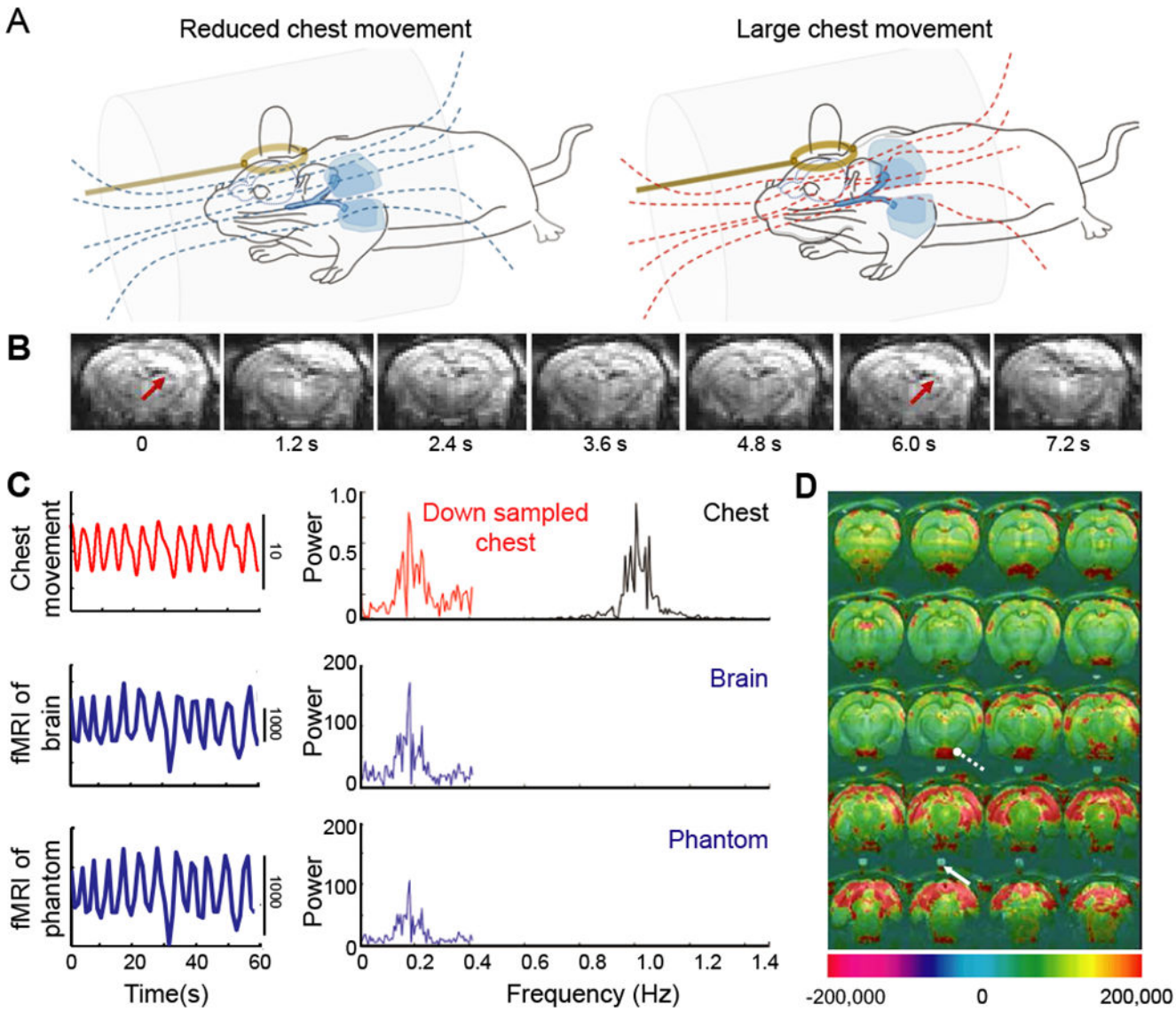

Figure 7. The aliasing effect of the respiratory-induced magnetic field (B_0) distortion.

(A) Schematic drawing of the B_0 field on free-breathing rats with different extents of chest movements and associated magnetic field lines. The distorted B_0 field is caused by the large chest movement during the respiratory cycles (red lines). Amber circles are pick-up coils. From (Pais-Roldan et al., 2018).

(B) The coronal sections from a three-dimensional echo-planar imaging sequence acquired at 1.2 s repetition time (TR), from 0 to 7.2 s, from a spontaneously breathing anesthetized rat. These data show the effect of the B_0-related motion artifacts at ~ 0.16 Hz as the function of time. From (Pais-Roldan et al., 2018).

(C) The respiratory trace (black, chest movement) and the down-sampled time course (red line) for a 1/TR sampling rate with TR = 1.2 s, upper panel). The power spectral density shows the aliased signal, peaked (f_{res} − 1/TR), i.e., 0.16 Hz, of which the f_{res} is around 1.0 ± 0.1 Hz. The fMRI time course and spectral density of a voxel in the brain (middle panel) or

in a phantom (bottom panel) over the animal's head shows the oscillatory signal with a bandwidth of 0.16 ± 0.1 Hz, which is dominated by the respiration-induced B_0 artifacts. The brain and phantom voxels are defined by the two arrows in panel D. From (Pais-Roldan et al., 2018).

(D) Map of the power at the artifact frequency, 0.16 ± 0.1 Hz shows the voxel-wise spatial correlation to the B_0-related artifacts. The high-power scales indicate the strong B_0-related artifacts. From (Pais-Roldan et al., 2018).

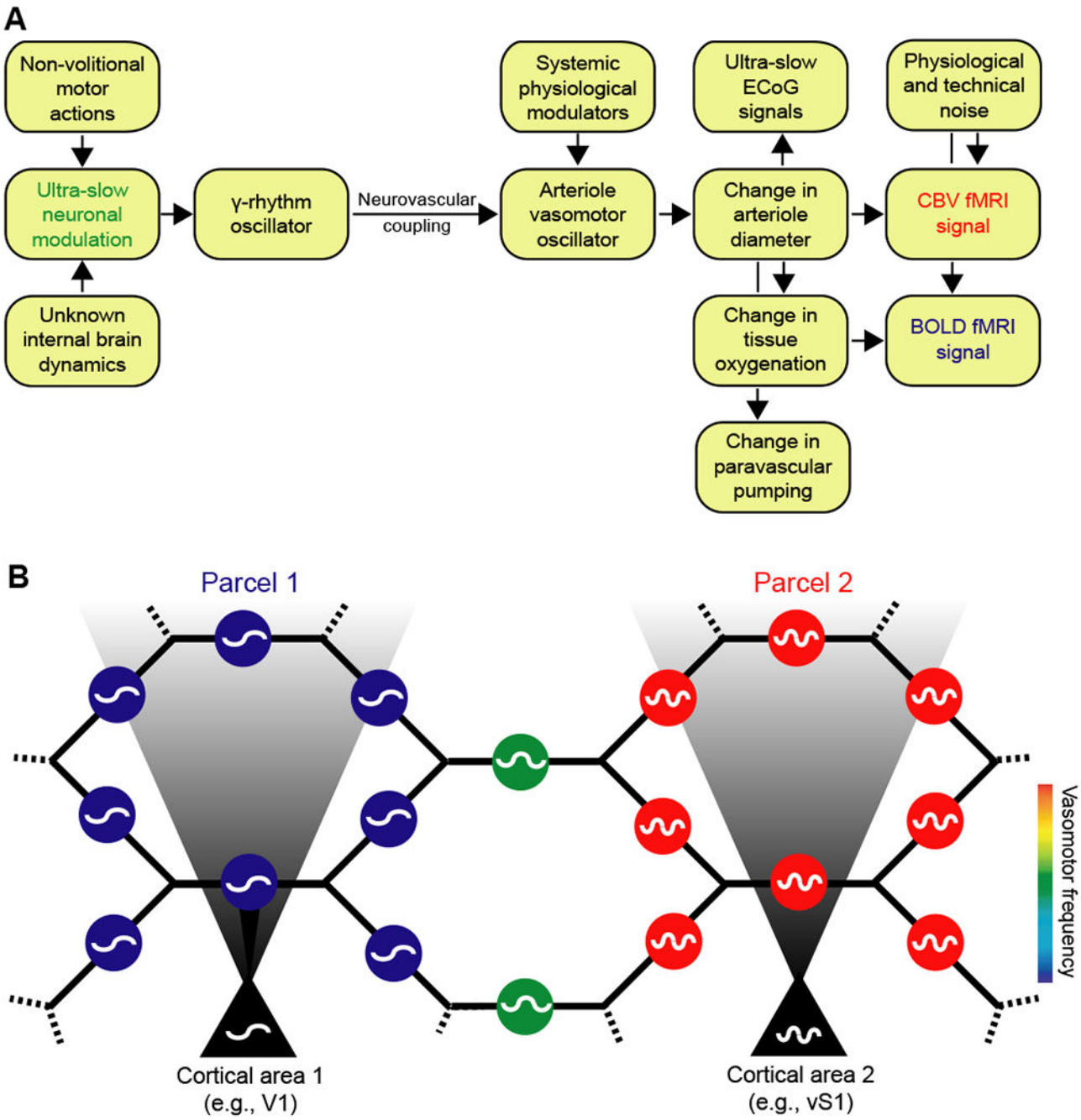

Figure 8. Coupled oscillator model for resting-state neurovascular coupling.

(A) Interactions for one region. Variations in γ-band electrical power lead to partial entrainment of the vasomotor oscillations in the smooth muscle of cortical surface and penetrating arterioles. Increases in γ-band electrical power dilate the arterioles and lead to an increase in the supply of fresh blood, as measured by CBV fMRI. The increase in diameter subsequently leads to an increase in blood oxygenation and a positive change in the BOLD fMRI signal. Coupling can be via callosal projections or via common input.

(B) Circuit of the pial arteriole network in terms of coupled smooth muscle oscillators. Each oscillator represents the activity of all muscles in one arteriole. The oscillators communicate with one another via the hexagonal lattice of electrically-joined endothelial cells that form the lumen (Fig. 6). Oscillators in a given region of the brain may also receive electrical input from underlying neuronal oscillators. This input can dominate and lead to a parcellation of the frequency of vasomotor oscillations, as observed by fMRI (Fig. 2B). Vasomotion is synchronous within a given region of the brain yet can occur with different frequencies in different regions; e.g., labeled blue and red for regions 1 and 2, respectively, and labeled green for an intermediate region without neuronal drive.